Tutor/s

Dr. Mohit Kumar
Departament de Química Inorgànica i Orgànica

Grau de Química

Treball Final de Grau

Controlling supramolecular organization and chiral assembly of functional molecules using heparin

Control de l'organització supramolecular i l'autoassemblatge quiral de molècules funcionals mitjançant heparina

Martí Torrades Violán

June 2025

UNIVERSITAT DE BARCELONA

B:KC Barcelona Knowledge Campus
Campus d'Excel·lència Internacional

En primer lloc, vull agrair al Dr. Mohit per haver estat al meu costat des del primer dia, ajudant-me i ensenyant-me tot allò que un es podria imaginar dins d'un laboratori. També per haver-me transmès la manera de pensar pròpia d'un investigador.

Al grup d'investigació, vull agrair especialment a la Dra. Poonam, per resoldre tots els dubtes que he tingut durant el projecte i per preocupar-se sempre per mi. També al Juan Carlos i la Sarah, per fer les hores de laboratori molt més entretingudes i divertides.

A la resta de companys amb qui vaig compartir inicialment el laboratori, el Toni, l'Arnau, la Yaiza i l'Oscar, que van acollir-me des del primer dia i es van preocupar per qualsevol inquietud meva. Encara que després canviéssim de laboratori, sempre em van deixar la porta oberta.

Així mateix, vull agrair al Josep la seva paciència per rebre cada dia moltes mostres meves per analitzar a l'HPLC-MS, així com per imprimir-me tots els resultats.

Finalment, no puc deixar d'agrair profundament als meus pares, que des de ben petit van despertar en mi un interés per la ciència i han estat una font d'inspiració constant. Sense vosaltres aquest treball no hauria estat possible. Gràcies per ser-hi sempre.

REPORT

IDENTIFICATION AND REFLECTION ON THE SUSTAINABLE DEVELOPMENT GOALS (SDG)

This project contributes to the achievement of Sustainable Development Goal (SDG) 3: Ensure healthy lives and promote well-being for all at all ages. The work focuses on the development of supramolecular assemblies based on achiral molecules capable of interacting with anionic biomolecules such as heparin, leading to the formation of helical nanostructures with potential applications in biomedical diagnostics.

Specifically, the project addresses the following SDG 3 targets:

Target 3.4: By 2030, reduce by one third premature mortality from non-communicable diseases through prevention and treatment, and promote mental health and well-being. The developed systems could serve as diagnostic tools to detect heparin levels in blood samples, helping to better monitor anticoagulant therapies and reduce complications related to thrombosis and cardiovascular diseases, major causes of premature mortality.

Target 3.8: Achieve universal health coverage, including access to safe, effective, quality, and affordable essential medicines and vaccines for all. The creation of affordable and sensitive diagnostic methods based on supramolecular sensors opens the possibility of implementing rapid testing technologies in resource-limited environments, thus promoting more equitable access to essential health care tools.

Target 3.d: Strengthen the capacity of all countries, in particular developing countries, for early warning, risk reduction, and management of national and global health risks. The research contributes to the advancement of biomedical diagnostic technologies, supporting the broader goal of strengthening health research capacity, particularly for non-communicable diseases.

This project primarily impacts the "People" pillar (one of the 5Ps of sustainable development), aiming to improve health outcomes and quality of life. If further developed, the supramolecular sensing platform could be adapted for the detection of other anionic biomolecules beyond heparin, expanding its applicability in preventive medicine and personalized health care.

CONTENTS

1. SUMMARY

The controlled assembly of π-conjugated molecules in water represents a key strategy in the development of functional supramolecular materials. This work presents the synthesis of a series of positively charged achiral molecules and explores their ability to self-assemble with negatively charged biomolecules, particularly heparin, in aqueous medium. The aim was to investigate how the binding of a biomolecule like heparin, along with other non-covalent interactions, drive the formation of functional supramolecular nanomaterials and how the chiral nature of heparin induces supramolecular chirality in the assembly of achiral molecular systems. The resulting supramolecular assemblies were characterized using ultraviolet-visible (UV-Vis) absorption, fluorescence, circular dichroism (CD) spectroscopies as well as transmission electron microscopy (TEM). We demonstrated that the binding of heparin resulted in the formation of helical nanostructures with distinct absorption and fluorescence properties and chiroptical activity. These findings demonstrate that the interaction between cationic achiral molecules and chiral polyanions not only enables the formation of well-defined nanostructures but also activates functional optical responses. It can be concluded that this strategy provides a promising platform for a) controlling supramolecular assembly of functional molecules; b) the design of responsive materials for the optical detection of biologically and biomedically relevant molecules.

Keywords: supramolecular polymers, non-covalent interactions, chiral induction, self-assembly, electrostatic interactions, helical nanostructures, π-conjugated systems, heparin sensing.

2. RESUM

L'assemblatge controlat de molècules π-conjugades en aigua representa una estratègia clau en el desenvolupament de materials supramoleculars funcionals. Aquest treball presenta la síntesi d'una sèrie de molècules aquirals amb càrrega positiva i explora la seva capacitat per autoassemblar-se amb biomolècules carregades negativament, en particular l'heparina, en medi aquós. L'objectiu era investigar com la unió amb una biomolècula com l'heparina, juntament amb altres interaccions no covalents, impulsa la formació de nanomaterials supramoleculars funcionals i com la naturalesa quiral de l'heparina indueix quiralitat supramolecular en aquests sistemes aquirals. Les estructures supramoleculars resultants es van caracteritzar mitjançant espectroscòpies d'absorció ultravioleta-visible (UV-Vis), fluorescència, dicroisme circular (CD), així com microscòpia electrònica de transmissió (TEM). Hem demostrat que la unió amb heparina dona lloc a la formació de nanoestructures helicoïdals amb propietats d'absorció i fluorescència distintives i activitat quiroòptica. Aquests resultats demostren que la interacció entre molècules aquirals catióniques i polianions quirals no només permet la formació de nanoestructures ben definides, sinó que també activa respostes òptiques funcionals. Es pot concloure que aquesta estratègia proporciona una plataforma prometedora per a: a) controlar l'autoassemblatge supramolecular de molècules funcionals; b) el disseny de materials sensibles per a la detecció òptica de molècules rellevants en contextos biològics i biomèdics.

Paraules clau: polímers supramoleculars, interaccions no covalents, inducció quiral, autoassemblatge, interaccions electrostàtiques, nanostructures helicoïdals, sistemes π-conjugats, detecció d'heparina.

3. INTRODUCTION

The precise control over the supramolecular organization of organic molecules is crucial for their application as functional nanomaterials. These assemblies rely on non-covalent interactions, such as hydrogen bonding, π-π stacking, hydrophobic effects and electrostatic interactions (Figure 1), to achieve significant control over molecular arrangement, enabling the emergence of new physicochemical properties and functions.[1,2]

Among organic systems, π-conjugated molecules are especially attractive due to their tunable optical and electronic characteristics. Their self-assembly has been widely explored in fields such as chemical sensing, diagnostics, organic electronics, organic photovoltaics, and drug delivery.[1,3] Importantly, controlling their organization in aqueous media opens the door to biocompatible applications, especially in biosensing and environmental monitoring.[2,4]

Naphthalene diimide (NDI) derivatives belong to a class of well-studied π-conjugated organic semiconductors. Their intrinsic planarity and strong π-π stacking affinity favor the formation of ordered supramolecular aggregates, which has facilitated its application in fields like printable electronics, analyte detection, fluorescence-based sensing, and diagnostic platforms.[3,5] Because of their potential applications, new designs of NDI-based supramolecular polymers are needed. More specifically, the NDIs that form functional nanostructures in aqueous medium will open doors to theranostic application.[6]

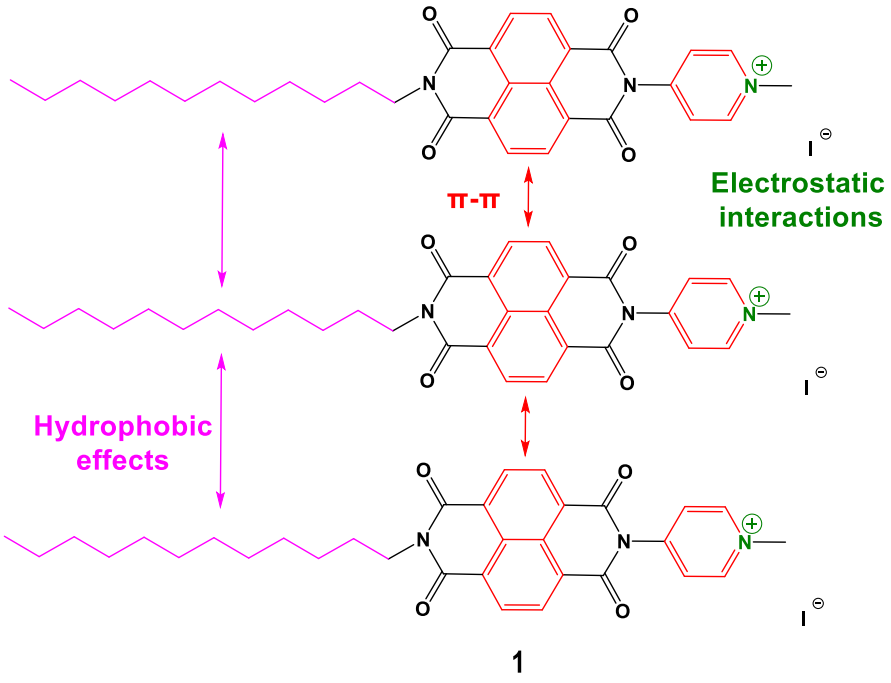

Figure 1. Types of non-covalent interactions of NDI-derivative **1**.

One strategy to regulate the assembly of NDI derivatives in water involves the interaction of NDI with biomolecules such as heparin. Heparin (Figure 2) is a natural, chiral biopolymer composed of repeating disaccharide units bearing sulfate and sulfonate groups, which confers it with a strong negative charge. Clinically, it plays an essential role as an anticoagulant and is routinely used to prevent clot formation during cardiovascular treatments and surgeries.

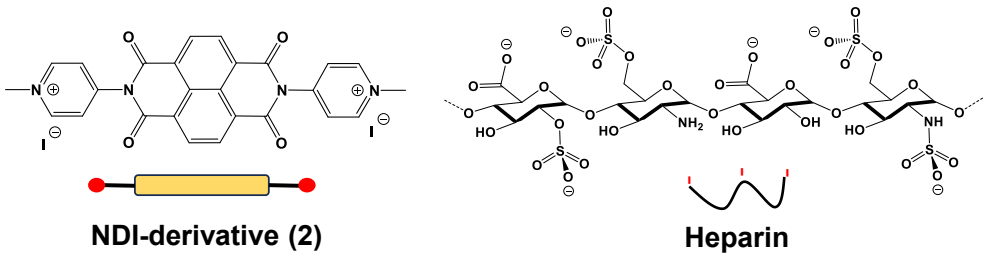

Figure 2. Molecular structures of NDI-derivative **2** and heparin.

Beyond its therapeutic relevance, heparin has emerged as a supramolecular tool to control organization due to its ability to interact with positively charged, achiral π-conjugated molecules. Through electrostatic interactions, it can induce aggregation of various cationic, π-conjugated molecules in aqueous media, whereas the inherent molecular chirality of heparin can also induce supramolecular chirality. This phenomenon, known as chirality induction, arises when chiral molecules such as heparin impose helical ordering into the assembly of achiral molecules (Figure 3). In supramolecular chemistry, this mechanism provides access to nanostructures with defined handedness and tunable optical properties, making it especially valuable for designing chiroptical materials and biosensing systems targeting biologically relevant anions.[2,4] Although NDI-based self-assembly has been extensively studied, the use of biomolecules such as heparin to control their supramolecular organization and helicity in aqueous media remains unexplored.

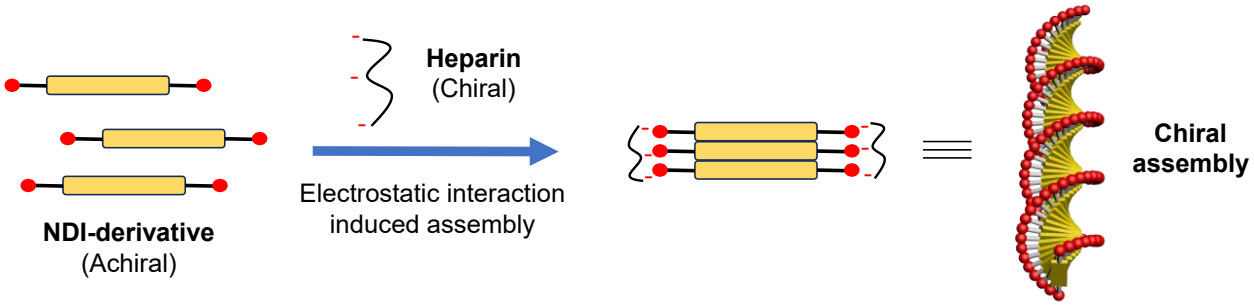

Figure 3. Schematic representation of heparin binding induced chiral self-assembly of achiral NDI-derivative.

This work investigates the self-assembly behavior of synthesized cationic NDI and naphthalene-based molecules in aqueous environments and their interaction with heparin, including the induction of chirality through electrostatic interactions. Using UV-Vis, fluorescence, CD spectroscopies as well as TEM, we analyze how these non-covalent interactions govern supramolecular organization. We demonstrate that heparin binding induces helical supramolecular organization of NDIs for future application as electronic nanomaterial, whereas the heparin responsiveness can have potential for bio-analyte sensing, targeting anionic biomolecules.

4. OBJECTIVES

The primary objective of this project is to develop heparin-responsive supramolecular polymers of NDI derivatives, and to investigate how their interaction with biomolecules like heparin can control their self-assembly.

The specific objectives are as follows:

• Synthesis of three positively charged, achiral molecules.

• Structural characterization of all obtained compounds by different techniques (TLC, ^{1}H and ^{13}C NMR, HPLC-MS).

• Explore the self-assembling properties of the positively charged achiral molecules in aqueous environments, particularly in the presence of polyanionic guests such as heparin.

• Assess whether the interaction with chiral anionic guests induces supramolecular helicity into the assembly of the achiral host molecule.

• Use optical techniques such as UV-Vis absorption, fluorescence, and CD spectroscopies, along with TEM, to investigate heparin binding and the assembly of the synthesized compounds.

5. RESULTS AND DISCUSSION

5.1. UNSUCCESSFUL REACTIONS

Several initial reactions were explored but did not yield the desired products. Details of these attempts, including experimental conditions, are provided in Appendix 1. Possible reasons for the failure are also discussed there.

5.2. SYNTHESIS OF ACHIRAL MOLECULE 1

A schematic summary of the reactions to synthesize the positively charged achiral molecule **1** will be discussed below (Scheme 1).

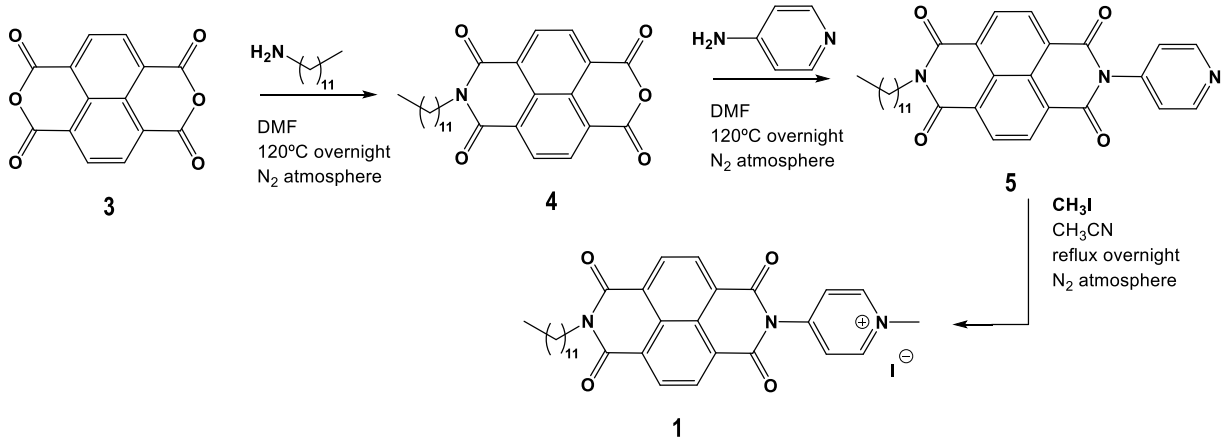

Scheme 1. Synthetic scheme of **1**.

5.2.1. Synthesis of N-dodecyl-1,4,5,8-naphthaleneimide (4)

The first reaction involved the preparation of N-dodecyl-1,4,5,8-naphthaleneimide (4), which was carried out by reacting 1,4,5,8-naphthalenetetracarboxylic dianhydride (3) with dodecylamine in dimethylformamide (DMF), leading to an imidation product. As shown in Scheme 2, the reaction gives rise to two products: the desired monofunctionalized compound **4** and the difunctionalized side product **4a**, which were separated by column chromatography.

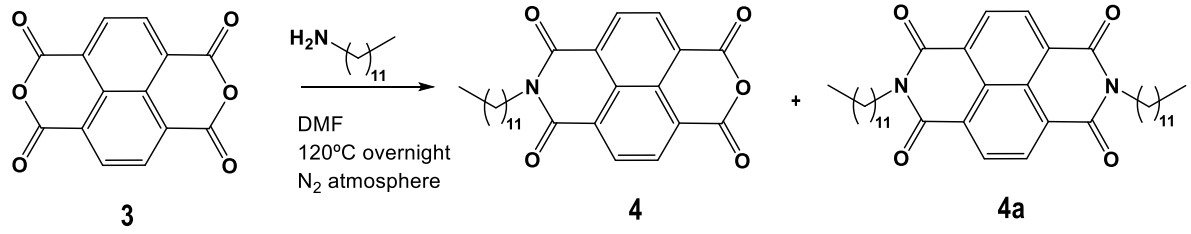

Scheme 2. Synthetic scheme of compound **4**.

The mechanism (Scheme 3) involves the nucleophilic attack of the amine nitrogen on the carbonyl carbon of the anhydride, forming a tetrahedral intermediate with a negatively charged oxygen and a positively charged nitrogen. The anhydride ring then opens, generating a carboxylic acid and an amide. Subsequently, the second carbonyl carbon can also be attacked intramolecularly by the amide nitrogen, although this nucleophile is weakened by resonance with the carbonyl. For this reason, high temperatures are required to complete the reaction. After the elimination of water as a leaving group, compound **4** is formed.

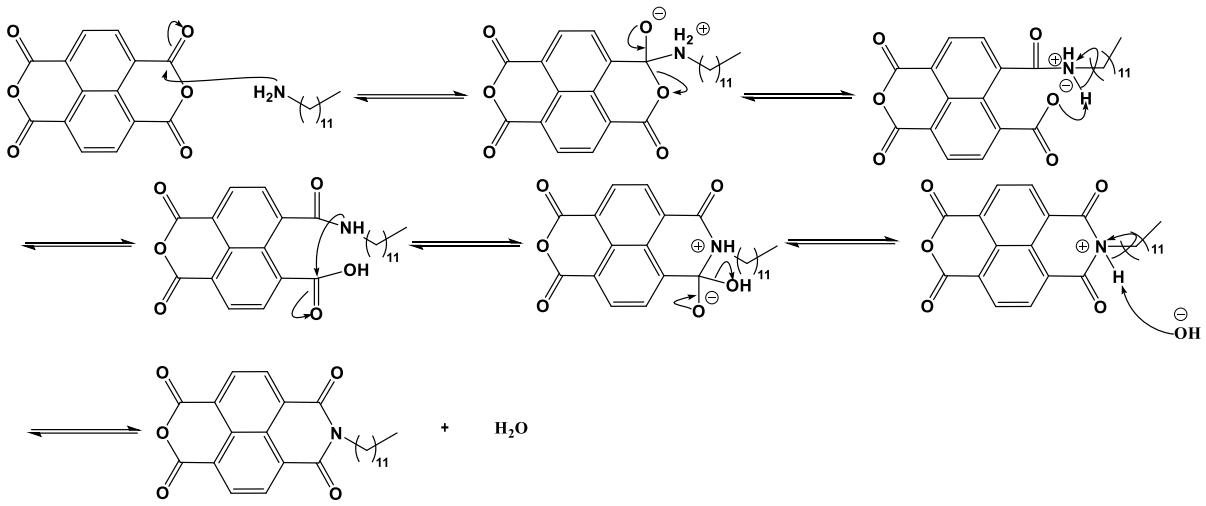

Scheme 3. Possible mechanism for the synthesis of compound **4**.

The overall yield was low (26%), likely due to a) the formation of the side product **4a**; b) the use of a non-dried solvent, which shifted the equilibrium towards the starting material because of the presence of water.

5.2.2. Synthesis of N,N'-pyridyl-dodecyl-1,4,5,8-naphthalenediimide (5)

The second reaction involved the preparation of N,N'-pyridyl-dodecyl-1,4,5,8-naphthalenediimide (5). This was achieved by reacting **4** with 4-aminopyridine, which attacks the remaining carbonyl group of the anhydride.

The overall yield was low (26%), mainly because we decided to avoid purification by column chromatography and instead attempt to purify the product via precipitation, filtration and washings. During this process, a lot of the product was lost in the filtrate.

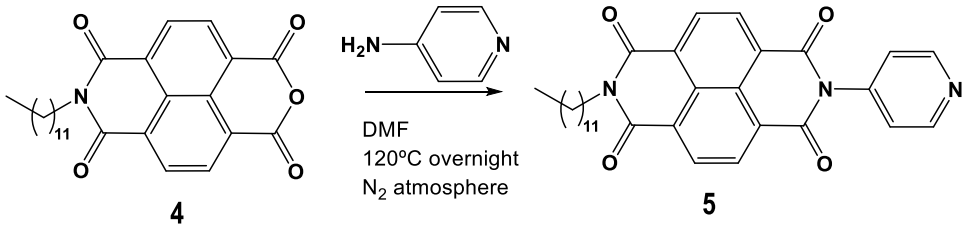

4 **5**

Scheme 4. Synthetic scheme of compound **5**.

The mechanism of the reaction is similar to what is described in Scheme 3 for the synthesis of **4**.

5.2.3. Synthesis of N,N'-methylpyridin-1-ium-dodecyl-1,4,5,8-naphthalenediimide (1)

The synthesis of **1** was performed by alkylation procedure with iodomethane (CH_3I) in acetonitrile (CH_3CN) under nitrogen (N_2) atmosphere.

The reaction was repeated because the initial crude product still contained traces of the reactant. To improve the conversion, the partially pure product was resubmitted to reaction conditions with excess CH_3I to fully alkylate the remaining reactant.

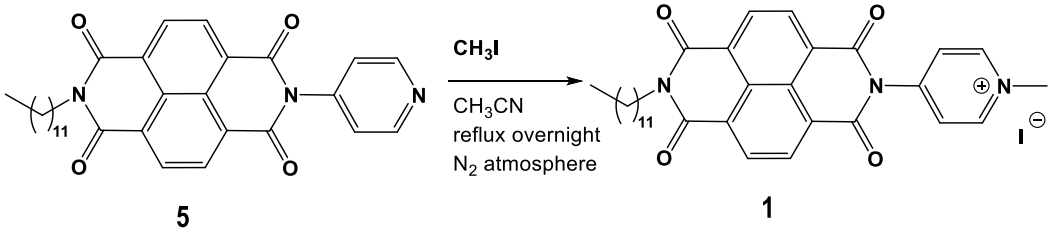

5 **1**

Scheme 5. Synthetic scheme of compound **1**.

The nitrogen atom of the pyridine undergoes a methylation reaction, where its lone pair attacks the electrophilic carbon of CH_3I, displacing the iodide as a leaving group via a possible S_N2 mechanism.

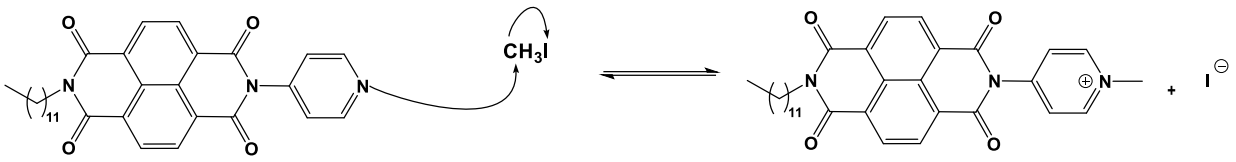

Scheme 6. Possible mechanism for the synthesis of compound **1**.

The resulting product features a twelve-carbon hydrophobic alkyl chain on one side and a quaternary ammonium group on the other, providing the molecule with distinct amphiphilic character, which is expected to self-assemble in water.

5.3. SYNTHESIS OF ACHIRAL MOLECULE 2

A schematic summary of the reactions to synthesize the two positively charged achiral molecule **2** will be discussed below (Scheme 7).

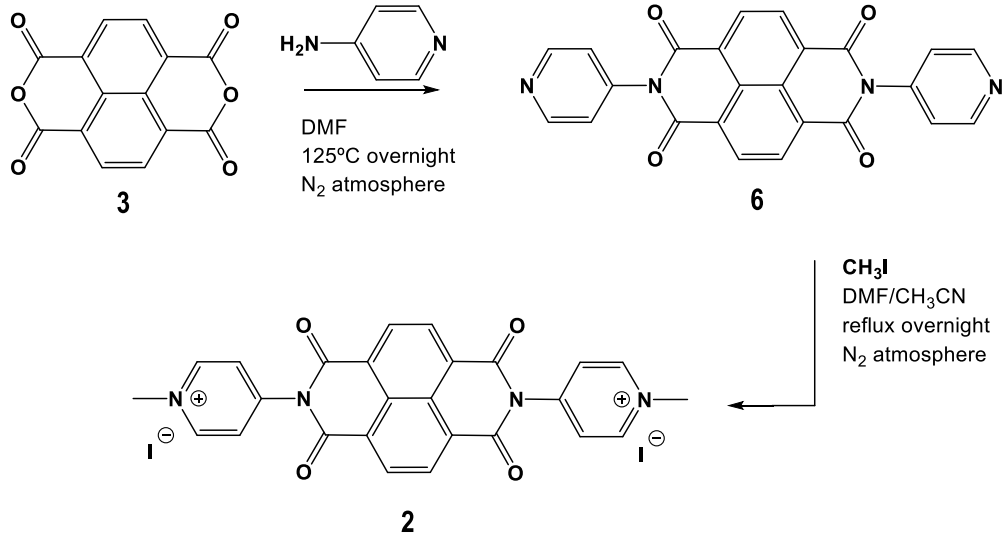

Scheme 7. Synthetic scheme of **2**.

5.3.1. Synthesis of N,N-di(4-pyridyl)-1,4,5,8-naphthalene (6)

The first reaction involved the preparation of **6**, which was carried out by reacting 1,4,5,8-naphthalenetetracarboxylic dianhydride (3) with 4-aminopyridine in dry DMF under N_2 atmosphere.[8]

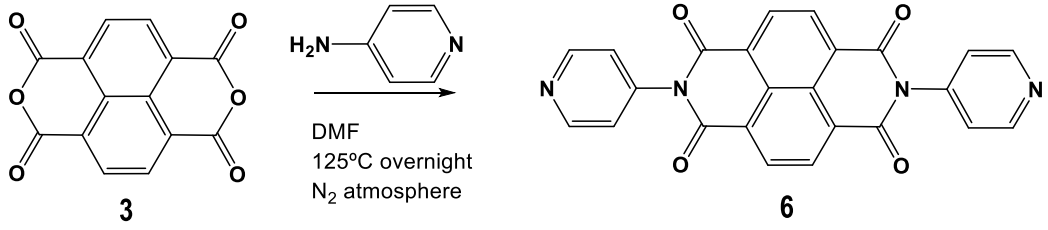

Scheme 8. Synthetic scheme of compound **6**.

Due to the use of an excess of 4-aminopyridine, several washing steps were required with cold DMF, water, acetone, and dichloromethane (CH_2Cl_2) to fully remove the unreacted amine. After washing, the crude product was recrystallized to eliminate any remaining impurities.

In this case, the yield was 54%, which, despite the reaction being very similar to the synthesis of compound **1**, is considerably higher. This increase is attributed to a) no possibility of the undesirable product; b) the use of dry solvent, which prevents the equilibrium from shifting toward the reactant by minimizing the presence of water. However, the overall yield was still moderate, as significant product losses occurred during the filtration and washing steps.

The mechanism of the reaction is similar to what is described in Scheme 3 for the synthesis of **4**.

5.3.2. Synthesis of Bis-N,Ń-(N-methylpyridin-1-ium)-1,4,5,8-naphthalenediimide iodide (2)

The synthesis of **2** was done by alkylation procedure with CH_3I in a mixed solution of CH_3CN and DMF (1:1, v/v) under N_2 atmosphere.[9] The reaction yields two products: the desired compound with methylation on both sides (95%) and a side product with methylation on only one side (5%).

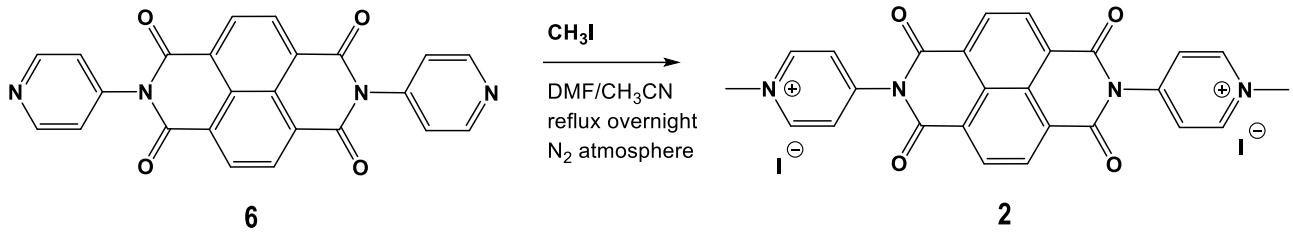

Scheme 9. Synthetic scheme of compound **2**.

The reaction was repeated because the initial crude product still contained traces of the monofunctionalized byproduct, which could interfere with subsequent studies. To improve the conversion, the partially pure product was subjected to the same reaction conditions with excess CH_3I to fully alkylate the remaining mono-substituted species.

After filtration, the resulting red solid was washed with CH_2Cl_2 and recrystallized from methanol (MeOH). Final analysis by ^1H NMR (Figure 20 in Appendix 2) confirmed the purity of the product to be 99%, with an isolated yield of 76.6%.

The mechanism of the reaction is similar to what is described in Scheme 6 for the synthesis of **1**.

5.4. Synthesis of achiral molecule 5-Methoxy-N,N,N-trimethyl-1-naphthalenammonium (8)

The synthesis of **8** was carried out via an alkylation reaction of 5-amino-1-naphthol (7) using excess CH_3I in CH_3CN, with an excess of potassium carbonate (K_2CO_3), under N_2 atmosphere.

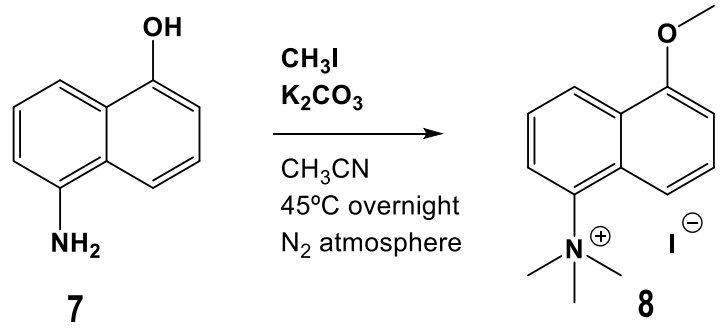

Scheme 10. Synthetic scheme of compound **8**.

The reaction proceeds via a possible S_N2 mechanism, following the same pathway as described in Scheme 6. The presence of K_2CO_3 is essential, as it serves to deprotonate both the amine and the phenolic hydroxyl group, enabling nucleophilic attack on the CH_3I.

After completion, the excess K_2CO_3 was removed by filtration, and the solvent was evaporated under reduced pressure. The resulting solid was washed with hexane and diethyl ether. Due to product loss during the filtration and washing steps, the final yield was a moderate 52%.

5.5 Binding with guest molecules

Once the described molecules were synthesized, the second objective of the project was to study how they self-assembled in different solvents. Specifically, their behavior was examined in various dimethylsulfoxide-water (DMSO-water) mixtures. This was followed by the investigation of the influence of heparin binding on the self-assembly of NDI and naphthalene derivatives. Finally, experiments were performed with chiral heparin molecule to observe induction of chirality.

5.5.1 UV-Vis absorption and fluorescence analysis of 1

The UV-Vis absorption and fluorescence spectroscopic changes provide crucial information about the formation of self-assembly. There are four main types of spectral signatures for the aggregation of π-conjugated molecules. First, scattering of light (at higher wavelengths) increases when the size of the molecular assemblies is comparable to the wavelength of light or higher. This is commonly observed in supramolecular polymers, which are much larger than monomers. Second, absorption band broadening occurs upon assembly. This is because monomers are homogeneous populations that absorb over narrow wavelength range, giving sharp, absorption bands, whereas aggregates are more heterogeneous, with variations in size and packing that broaden the absorption spectral features. Third, absorbance decreases, because a) the molar extinction co-efficient of aggregates are known to be lower that monomers; b) fewer molecules absorb at exactly the same wavelength, reducing the overall signal. In the emission, we can have either shift of emission band, fluorescence quenching or even appearance of new emission band upon self-assembly. Finally, supramolecular polymers can form either J-aggregates (red shifted) or H-aggregates (blue shifted), leading to shift in spectral band position and that can result in changing the relative ratios of the absorption band as one type of aggregates dominate over the other.

The chemical design of **1** resembles like an amphiphile and is expected to self-assemble in water. The spectroscopic analysis of **1** in DMSO-water mixtures enabled the evaluation of its self-assembly behavior as a function of water content and upon heparin binding. As shown in Figure 4a, at low water percentages, the spectra exhibit features which are associated with predominantly monomeric state. This includes sharp absorption bands at 360 and 380 nm, with no scattering signal at higher wavelengths. As the water content increases (≥ 70%), notable spectral changes such as band broadening, increase in the scattering of light and slight red shifts were observed. These changes are consistent with the formation of self-assembly, driven by hydrophobic and π-π interactions. At high water content (90-99%), **1** self-assembles even in the absence of heparin.

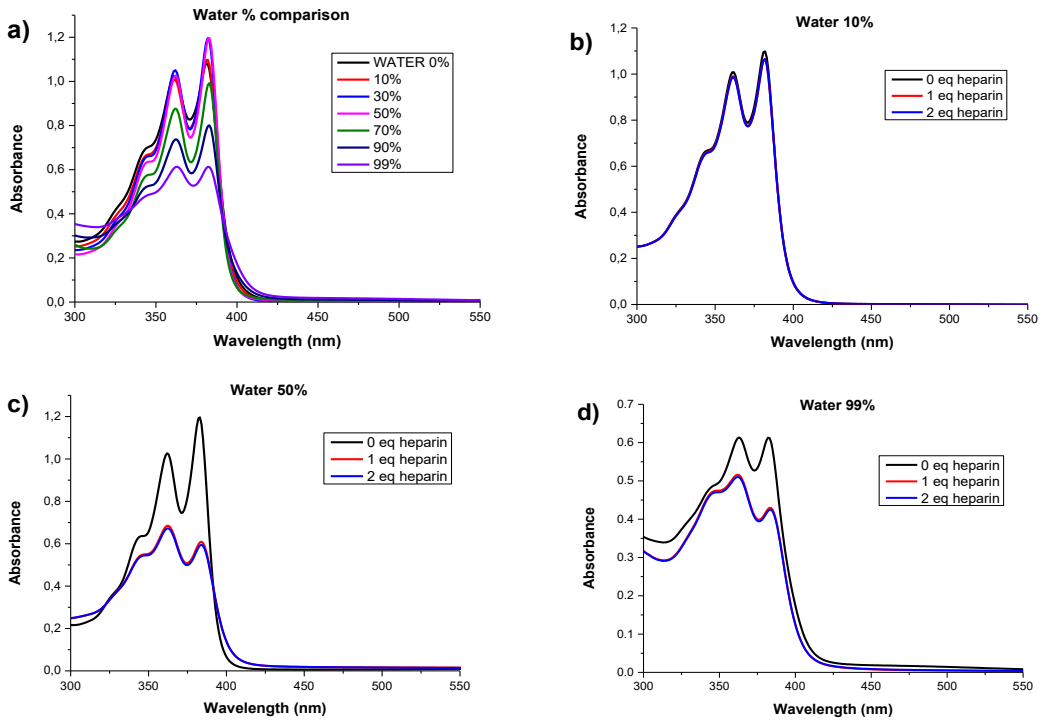

Figure 4. UV-Vis absorption spectra of **1** (0.05 mM) (a) in varying % of water in DMSO, (b) 10% water, (c) 50% water and (d) 99% water with one and two molar equivalents of heparin. Since heparin is a polymer, equivalents of heparin are basically molar equivalents of individual monosaccharide units with the assumption that each monosaccharide contains one anionic site.

The addition of heparin markedly influenced the system. As shown in Figure 4b, at low water percentages, no change was observed upon heparin addition, as the system remains mostly monomeric and the electrostatic interaction with heparin alone was insufficient to induce self-assembly of NDI. In contrast, at higher water percentages like 50% water, introducing one molar equivalent of heparin leads to significant spectral changes, indicating the formation of supramolecular aggregates through electrostatic interactions between the cationic groups of **1** and the anionic groups of heparin. Importantly, beyond one equivalent, no further spectral variation was

observed, indicating saturation of the binding sites on **1** through 1:1 binding, which is theoretically expected. It confirms the efficient interaction between the two components under the tested conditions.

The titration of **1** with increasing heparin equivalents in 50% and 99% water shows distinct aggregation behavior. In 50% water, heparin gradually promotes self-assembly as seen by the broadening of the absorption spectra and the change in the ratio of the absorption band (Figure 5a) along with increase in the scattering signal at *e.g.* 500 nm. However, in 99% water, the molecules are already highly aggregated due to hydrophobic and π-π interactions, and just 0.1 equivalents of heparin are sufficient to reach saturation, with heparin binding inducing minimal further change.

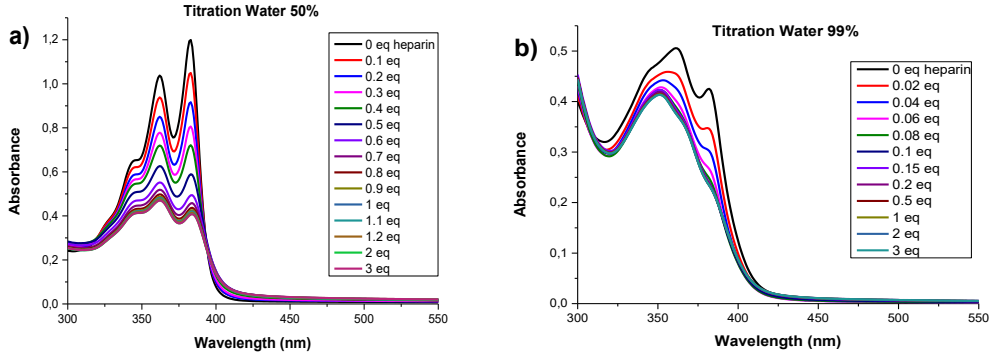

Figure 5. UV-Vis absorption spectra of **1** (0.05 mM) upon addition of varying equivalents of heparin (a) in 50% water and (b) in 99% water.

The fluorescence spectra presented in Figure 6 provide key insights into the behavior of **1** in different DMSO-water mixtures and upon binding with heparin.

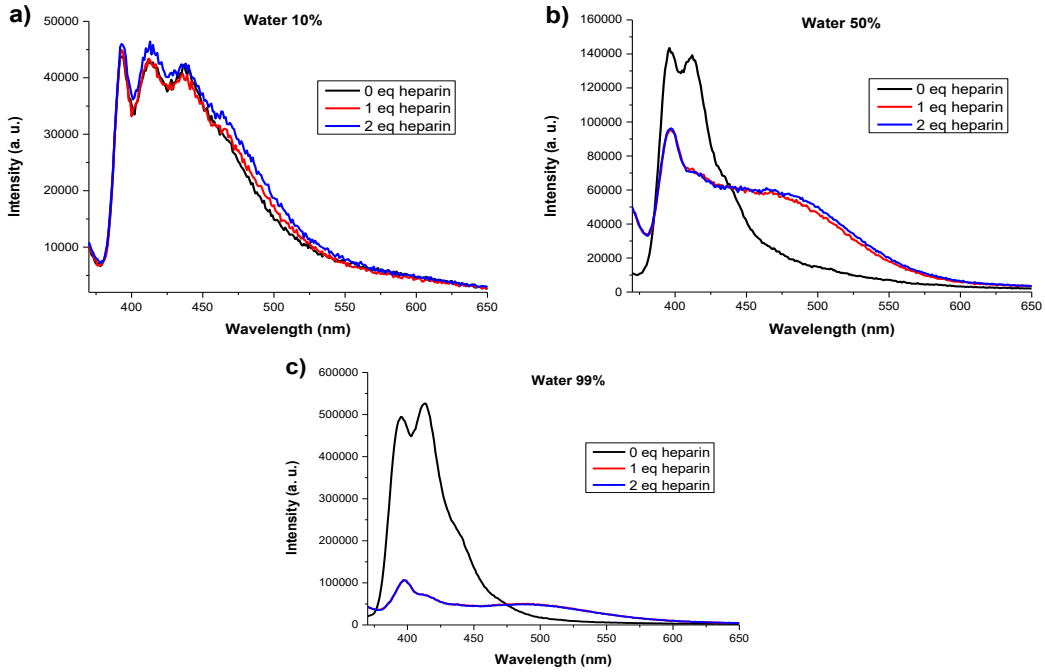

Figure 6. Fluorescence spectra of **1** (0.05 mM) in (a) 10% water, (b) 50% water and (c) 99% water with one and two equivalents of heparin.

As shown in figure 6, the fluorescence behavior is in line with the UV-Vis results, confirming aggregate formation as seen by decrease in the monomeric emission intensity and the emergence of a new, weakly emitting band at around 500nm (Figure 6b, 6c). Such a new emission band has been assigned to the formation of NDI excimer, i.e. excited state dimer.[10] Consistent with the absorption studies, at low water content like 10% water, the addition of heparin has no significant effect, whereas at high water content clear effects are observed. This is because heparin binding alone cannot induce self-assembly of **1** at low water percentages, while at high water content the increased hydrophobic effects promote aggregation, and the addition of heparin further facilitates this process through electrostatic interactions.

5.5.2 UV-Vis absorption and fluorescence analysis of 2

The spectroscopic analysis of **2** in DMSO-water mixtures reveal a self-assembly behavior notably different from **1**. While **1** tends to aggregate at high water content, **2** remains mostly monomeric under these conditions and instead shows greater aggregation at lower water percentages.

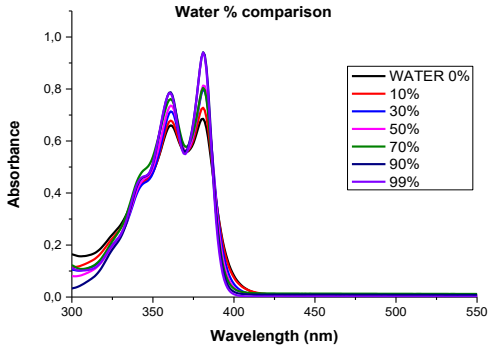

Figure 7. UV-Vis absorption spectra of **2** at various percentage of water in DMSO.

This difference is attributed to their distinct structures: **1** contains a hydrophobic chain that promotes aggregation in water, whereas **2** carries two positive charges, enhancing its solubility in water but reducing it in DMSO, leading to aggregation in the latter.

Despite these differences, both compounds exhibit similar responses to heparin. As shown in Figure 8, the addition of one equivalent of heparin induces supramolecular aggregation. However, in the case of **2**, further spectral changes are observed beyond this point, suggesting that saturation is not reached, due to the presence of two positive charges.

Interestingly, at low water content, heparin addition has no observable effect. While this parallels the behavior of **1**, the underlying reason may be slightly different. In **1**, heparin alone cannot induce aggregation in a fully monomeric system. For **2**, although aggregation occurs at low water percentages, the positive charges are expected to be buried within the aggregates, making them inaccessible for heparin interaction. In contrast, at high water content, the positive charges are exposed on the aggregate surface, allowing effective electrostatic interaction with heparin, which explains the clear changes observed at higher water percentages.

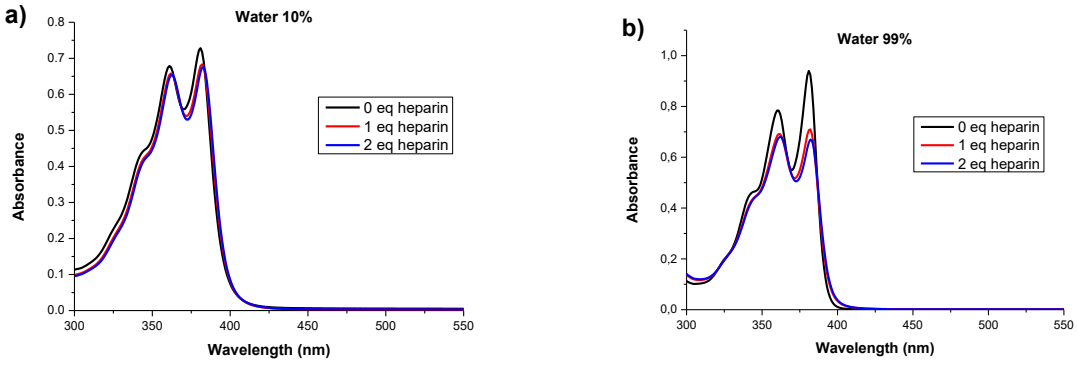

Figure 8. UV-Vis absorption spectra of **2** (0.05 mM) with one and two equivalents of heparin in (a) 10% water and (b) 99% water.

The fluorescence spectra in Figure 9 provide valuable insights into the behavior of **2** in DMSO-water mixtures and its interaction with heparin.

The emission data is consistent with the UV-Vis results, confirming aggregation through decreased monomeric emission. At high water content, the system shows higher emission intensity with sharp peaks at 390 and 410 nm, reflecting a more monomeric state (Figure 9a). As the water content decreases, we observe a decrease in monomeric emission intensity indicating aggregation of **2**. Similarly, the addition of heparin has little effect at low water percentages (10% water) but induces clear changes through decreased monomeric emission at high water content (99% water).

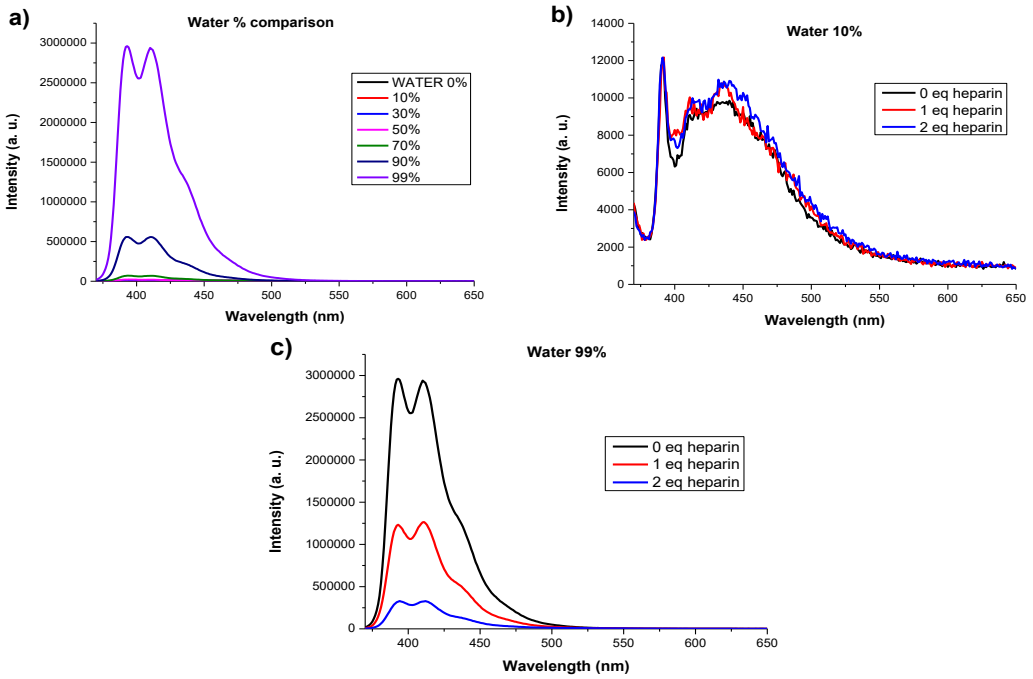

Figure 9. Fluorescence spectra of **2** (0.05 mM) in (a) various water %, (b) 10% water and (c) 99% water with one and two equivalents of heparin.

The addition of increasing amounts of heparin to **2** in 99% water (Figure 10) reveals a progressive self-assembly process. Without heparin, the UV-Vis and fluorescence spectra display sharp peaks typical of the monomeric form. As heparin is added, the intensity of these peaks gradually decreases, indicating the self-assembly of **2**. This aggregation is induced by the electrostatic interactions between the cationic groups of **2** and the anionic groups of heparin, complemented by π-π stacking between the NDI chromophores.

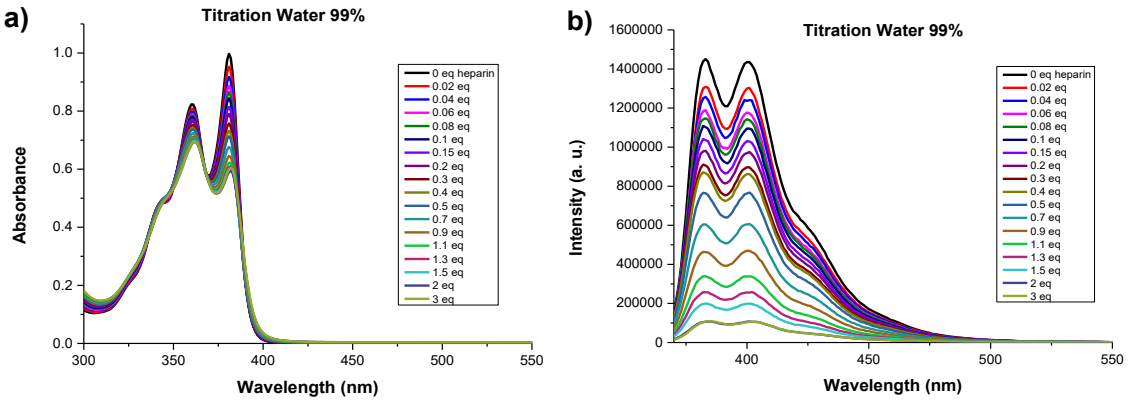

Figure 10. Variation in the (a) UV-Vis absorption spectra and (b) fluorescence spectra of **2** (0.05 mM) in 99% water upon addition of increasing amounts of heparin.

5.5.3 UV-Vis absorption and fluorescence analysis of 8

The naphthalene derivative (8) has a distinct spectral pattern compared to NDI, and we aimed to investigate how this difference affects its self-assembly behavior and interaction with heparin. The same set of experiments described for **1** and **2** were carried out, including the comparison of different DMSO-water mixtures and their response to heparin addition.

As shown in Figure 11a, the solvent mixture comparison reveals minor spectral changes, making it difficult to determine whether aggregation occurs. Notably, at low water content (0-10%), a small band appears at 375 nm, which might be attributed to intramolecular charge transfer between the methoxy group and the quaternary amine. However, further studies are needed to confirm this.

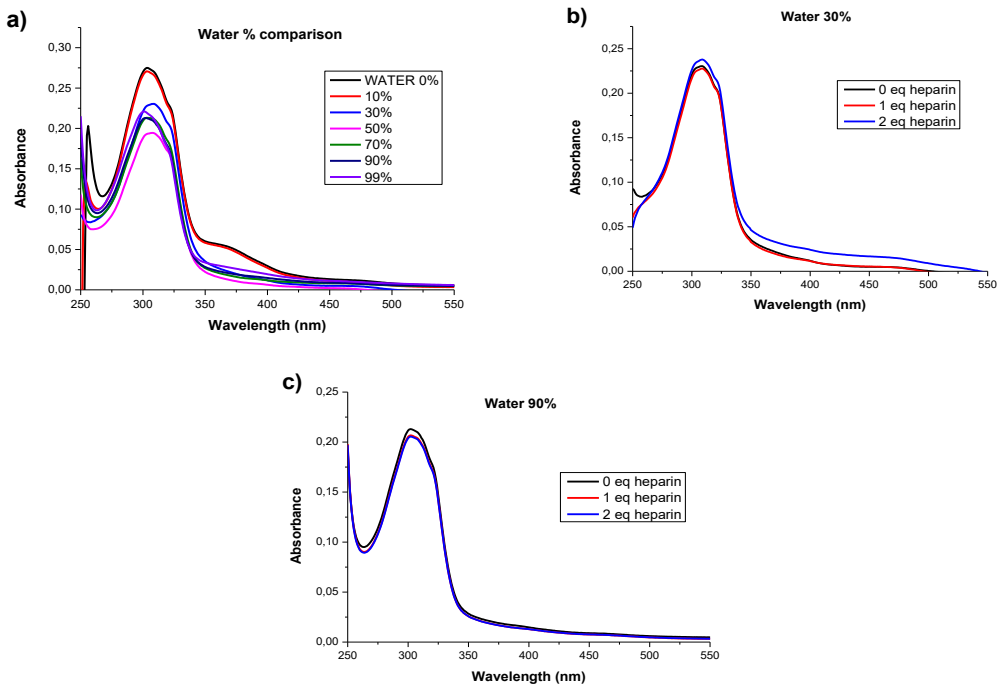

Figure 11. UV-Vis absorption spectra of **8** (0.1 mM) in (a) various water %, (b) 30% water and (c) 90% water with one and two equivalents of heparin.

In the case of **8**, we observe that neither at low nor high water percentages do the addition of heparin produce significant changes, indicating that heparin does not alter the structure or induce aggregation.

Fluorescence results closely match the UV-Vis data, confirming the same conclusions. No notable changes are seen upon adding heparin at different water ratios. However, we do observe variations in emission intensity across solvent mixtures, with an increase at higher water content followed by a decrease around 50%, suggesting that aggregation might be favored in mixed solvents. Again, further studies would be required to confirm this phenomenon.

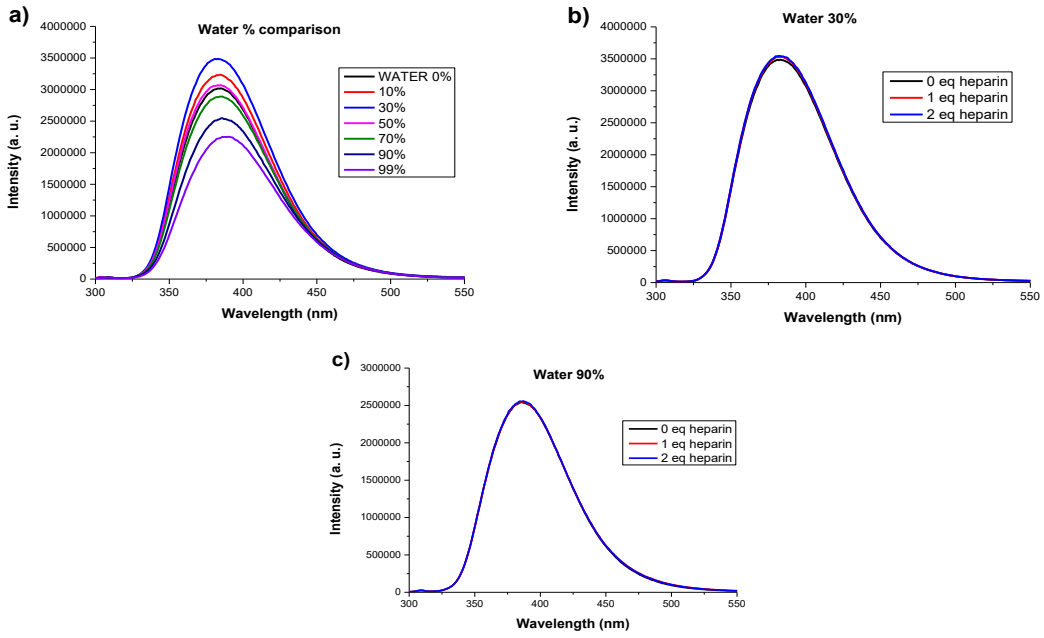

Figure 12. Fluorescence spectra of **8** (0.1 mM) in (a) various water %, (b) 30% water and (c) 90% water with one and two equivalents of heparin.

Overall, based on these studies, we conclude that **8** shows no clear spectroscopic evidence of aggregate formation and heparin binding, likely due to its structural characteristics. Unlike NDI, the naphthalene core has a smaller π-cloud, which may reduce its propensity for self-assembly. However, further experiments will be needed to confirm these conclusions.

5.5.4 Heparin binding induced supramolecular chirality in 1 and 2 self-assembly

After confirming the heparin binding induced supramolecular transformation, we next probed the ability of heparin to induce chiral organization into the assembly of achiral **1** and **2**.

Derivative **2** is molecularly achiral, and therefore, its self-assembly in 99% water does not show any CD signal (Figure 13a), indicating achiral or racemic organization. However, binding of heparin, as the chiral guest molecule, to self-assembled **2** is expected to result in a chiral complex with a defined CD signal. We observed a well-defined negative bisignated CD signal with a negative maximum at 410 nm followed by a positive maximum at 360 nm. This confirms that the heparin binding induced an excitonic coupling of the NDI chromophores of **2** resulting in a left-handed helical assembly.[2]

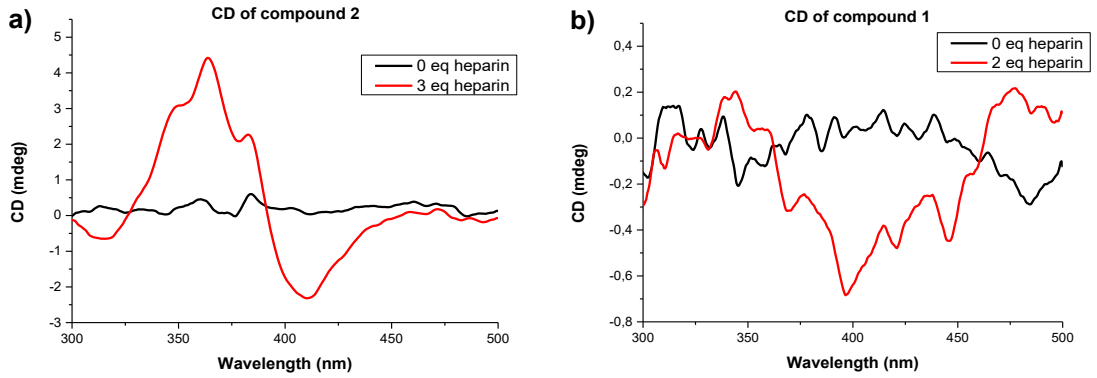

Figure 13. CD spectrum of a solution of (a) **2** (0.1 mM) in 99% water upon heparin binding; (b) **1** (0.05 mM) in 50% water upon heparin binding.

In contrast, the CD spectrum of compound **1** in 50% water with two equivalents of heparin (Figure 13b) do not show a bisignated signal, likely due to a smaller aromatic core. **2** may be more effective in forming stable helical structures due to its larger aromatic core, which can enhance π-π stacking interactions and overall supramolecular stability. Previous results from the group have shown that the doubly charged NDI, without additional aromatic units like pyridine, do not show any CD signal upon binding with heparin. This indicates that the ability of **2** to show heparin binding induced CD signal is most likely driven by the additional aromatic interaction provided by the two pyridine units.

5.5.5 Transmission Electron microscopy (TEM) of 2

Until now, we have shown that heparin successfully binds to the self-assembled and monomeric form of **2**, which results in spectroscopic changes that indicate supramolecular reorganization. We next used TEM to understand the morphological transformation associated with heparin binding. Thus, a sample of **2** in 99% water with heparin, was drop-casted and dried on a TEM copper grid. The sample was stained with uranyl acetate to improve contrast and to facilitate TEM imaging. TEM micrographs of the sample clearly show the formation of 2-dimensional sheet-like structures (Figure 14). These indicates well-defined organization of NDI molecules upon binding with heparin. Although the resolution of the image was not sufficient to obtain further molecular packing details, we expect the NDIs to be organized in a way such that the positively charged, heparin bound units are positioned on both faces of the sheet.[2]

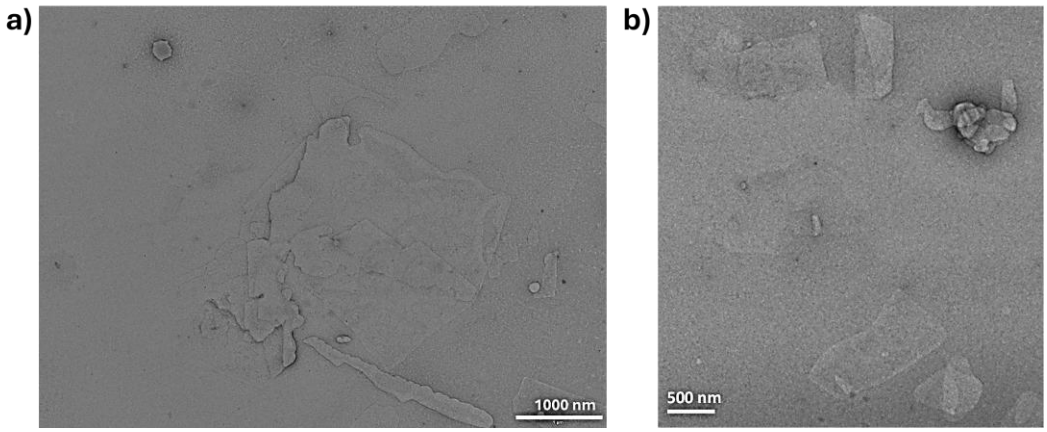

Figure 14. TEM images in the presence of heparin showing heparin-induced self-assembly of **2** (a), and (b) is a higher resolution image of this sample in another area.

6. EXPERIMENTAL SECTION

6.1 MATERIALS AND METHODS

The described reactions were carried out inside fume hood, using an aluminum heating block and a magnetic stirrer for all of them. All reagents employed were obtained from commercial suppliers.

Thin-layer chromatography (TLC) was performed on Merck silica gel 60 F254 aluminum plates, with detection under UV light. When the compounds were not UV-active, visualization was achieved by exposing the plates to iodine, which reacts with specific functional groups and produces visible spots. Additionally, the ninhydrin test was used to detect primary and secondary amines, providing further confirmation of amine functionality in the samples.

Column chromatography was performed over silica gel.

NMR spectra were recorded using a Bruker Mercury 400 spectrometer, with frequencies of 400 MHz for ^{1}H and 101 MHz for ^{13}C. Chemical shifts (δ) are expressed in ppm, and tetramethylsilane (TMS) was used as the internal reference standard for the calibration of chemical shifts in NMR spectroscopy. The TMS signal corresponds to a singlet (δ 0.00). In the ^{1}H NMR spectra, solvent peaks appear at δ 2.5 for deuterated dimethylsulfoxide (DMSO d^6) and δ 7.26 for deuterated chloroform ($CDCl_3$), while in the ^{13}C NMR spectrum, the DMSO d^6 and $CDCl_3$ solvent peaks appears at δ 40 and 77 respectively.

Samples of 2.5 mL were placed in 1 cm path length cuvettes for spectroscopic measurements. Glass cuvettes were used for **1** and **2**, while quartz cuvettes were used for **8**. UV-Vis absorption spectra were recorded using an Agilent Cary 5000 spectrophotometer at a scanning speed of 600 nm/min. The measurement range was 300-600 nm for **1** and **2** and 250-600 nm for **8**.

Fluorescence spectra were measured using a Photon Technology International fluorimeter equipped with a xenon arc lamp. The same cuvette setup was used as for the absorbance measurements. Excitation wavelengths were set at 350 nm for **1** and **2** and 280 nm for **8**.

The CD spectra were recorded using a Jasco J-815 spectropolarimeter (Serial no. A009761168) with a wavelength range of 290-500 nm. Sample solutions were prepared at a concentration of 0.05 mM in different water ratios in DMSO and placed in a glass cuvette with a path length of 1 cm. Spectra were recorded at a scan speed of 200 nm/min. Data analysis included baseline correction by subtracting the blank solution. The data was smoothened using 12 points of Adjacent-Averaging method.

The TEM images were recorded on a Jeol J1010 microscope operating at an accelerating voltage of 80 kV. The samples for TEM analysis were prepared by drop casting 10 µL aliquot of the sample solution on a carbon film grid (400 mesh, copper) and dried for two minutes. Then excess sample solution was wicked off with filter paper and dried completely. Then, 10 µL uranyl acetate stain (2% solution) was drop casted, blotted away after 30 seconds, and dried completely. The grid was then air dried at room temperature overnight before imaging.

6.2 SYNTHESIS OF ACHIRAL MOLECULE 1

6.2.1 Synthesis of N-dodecyl-1,4,5,8-naphthaleneimide (4)

A solution of 1,4,5,8-naphthalenetetracarboxylic dianhydride (3) (2.00 g, 7.46 mmol) in DMF (70 mL) was heated at 120 °C for 30 minutes. Separately, dodecylamine (1.38 g, 7.46 mmol) was dissolved in DMF (40 mL) and added dropwise to the preheated solution. The reaction mixture was stirred at 120 °C under N_2 atmosphere overnight.

After 24 hours, the mixture was poured into water to precipitate the product, which was collected by filtration and washed with water. The crude solid was purified by column chromatography, eluting with CH_2Cl_2/hexane (7:3), gradually increasing to 100% CH_2Cl_2.

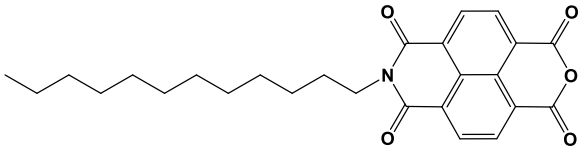

Yellow-white solid. Yield: 26% (0.838 g). ^{1}H NMR ($CDCl_3$, 400 MHz): δ 8.82 (s, 4H), 4.20 (t, J = 7.6 Hz, 2H), 1.74 (p, J = 7.5 Hz, 2H), 1.30 (m, 18H), 0.88 (t, J = 6.7 Hz, 3H).

6.2.2 Synthesis of N,N'-pyridyl-dodecyl-1,4,5,8-naphthalenediimide (5)

A solution of N-dodecyl-1,4,5,8-naphthaleneimide (4) (0.10 g, 0.23 mmol) and 4-aminopyridine (0.19 g; 2 mmol) was dissolved in DMF (10 mL) and heated at 120ºC under N_2 atmosphere overnight. After cooling to room temperature, the reaction mixture was filtered, and the solid was washed with cold DMF, water and diethyl ether (50 mL of each).

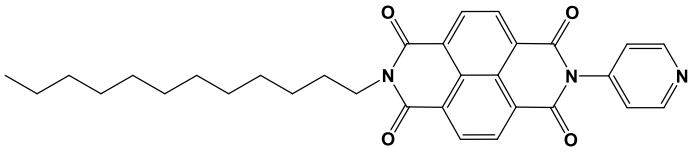

Yellow-white solid. Yield: 26% (31 mg). ^{1}H NMR ($CDCl_3$, 400 MHz): δ 8.89 (dd, J = 4.8, 1.6 Hz, 2H), 8.83 (s, 4H), 7.49 (d, J = 5.0 Hz, 2H), 4.22 (t, J = 7.6 Hz, 2H), 1.77 (p, J = 7.4 Hz, 2H), 1.30 (m, 18H), 0.88 (t, J = 6.7 Hz, 3H). ^{13}C NMR ($CDCl_3$, 101 MHz): 162.60, 162.30, 142.90, 131.70, 131.10, 127.40, 127.10, 126.90, 126.10, 124.00, 41.15, 32.95, 29.66, 29.64, 29.60, 29.54, 29.36, 29.33, 28.10, 27.10, 22.75, 14.20. HPLC-MS: m/z calc for $C_{31}H_{33}N_3O_4$ $[M+H]^+$ 512.612; found 512.2.

6.2.3 Synthesis of N,N'-methylpyridin-1-ium-dodecyl-1,4,5,8-naphthalenediimide (1)

A solution of N,N'-pyridyl-dodecyl-1,4,5,8-naphthalenediimide (5) (25 mg, 0.05 mmol) and CH_3I (high excess) was dissolved in CH_3CN (10 mL) and refluxed under N_2 atmosphere overnight. After cooling to room temperature, the reaction mixture was filtered, and the orange solid was washed with diethyl ether.

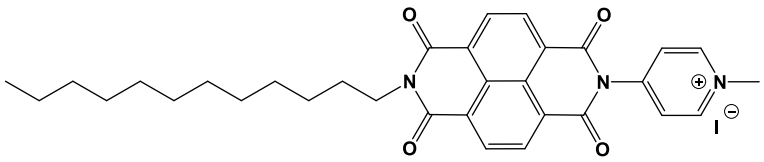

Orange solid. Yield: 85% (22 mg). ^{1}H NMR (DMSO d^6, 400 MHz): δ 9.21 (d, J = 6.9 Hz, 2H), 8.75 (s, 4H), 8.31 (dd, J = 5.0, 2.0 Hz, 2H), 4.45 (s, 3H), 4.08 (t, J = 7.4 Hz, 2H), 1.68 (p, J = 7.58 Hz, 2H), 1.30 (m, 18H), 0.85 (t, J = 6.7 Hz, 3H). ^{13}C NMR (DMSO d^6, 101 MHz): 163.00, 162.65, 150.90, 147.75, 131.35, 130.95, 129.00, 127.60, 127.05, 126.80, 126.55, 48.75, 31.80, 29.51, 29.47, 29.45, 29.37, 29.21, 29.18, 27.85, 27.00, 22.50, 14.50. HPLC-MS: m/z calc for $C_{32}H_{36}N_3O_4^+$ 526.638; found 526.2.

6.3 SYNTHESIS OF ACHIRAL MOLECULE 2

6.3.1 Synthesis of N,N-di(4-pyridyl)-1,4,5,8-naphthalene (6)

N,N-di(4-pyridyl)-1,4,5,8-naphthalene (6) was synthesized according to previous methods with some modifications.[8] 1,4,5,8-Naphthalenetetracarboxylic dianhydride (3) (0.50 g; 1.86 mmol), 4-aminopyridine (0.57 g; 6 mmol), and dry DMF (20 mL) were heated at 125ºC for 24 h under N_2 atmosphere. After cooling to room temperature, the reaction mixture was filtered, and the solid was washed with cold DMF, water, acetone, and CH_2Cl_2 (50 mL of each). **6**, as a gray-white solid was obtained by recrystallization with DMF.

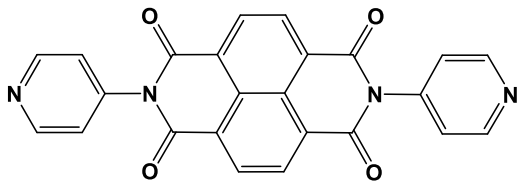

Gray-white solid. Yield: 54% (0.425 g). ^{1}H NMR (DMSO d^6, 400 MHz): δ 8.82 (dd, J = 4.5, 1.6 Hz, 4H), 8.75 (s, 4H), 7.58 (dd, J = 4.4, 1.6 Hz, 4H). HPLC-MS: m/z calc for $C_{24}H_{12}N_4O_4$ $[M+H]^+$ 421.384; found 421.1.

6.3.2 Synthesis of Bis-N,Ń -(N-methylpyridin-1-ium)-1,4,5,8- naphthalenetetracarboxylic diimide iodide (2)

2 was synthesized according to previous methods with some modifications.[9] N,N-di(4-pyridyl)-1,4,5,8-naphthalene (6) (0.20 g; 0.48 mmol) was dissolved in a mixed solution of CH_3CN and DMF (1:1, v/v), to which CH_3I (120 µL; 1.9 mmol) solution in CH_3CN was

added dropwise. The mixture was refluxed for 24 h under N_2 atmosphere, cooled to room temperature, filtered, and washed with CH_2Cl_2. The red solid product was obtained by recrystallization from MeOH.

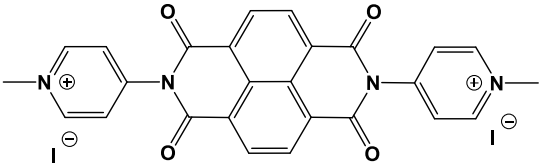

Red solid. Yield: 77% (0.164 g). ^{1}H NMR (DMSO d^6, 400 MHz): δ 9.23 (d, J = 6.9 Hz, 4H), 8.82 (s, 4H), 8.33 (dd, J = 6.9 Hz, 4H), 4.47 (s, 6H). HPLC-MS: m/z calc for $C_{26}H_{18}N_4O_4^{2+}$ 225.222; found 225.2

6.4 Synthesis of achiral molecule 5-Methoxy-N,N,N-trimethyl-1-naphthalenammonium (8)

A solution of 5-amino-1-naphthol (7) (0.20 g; 1.25 mmol), CH_3I (3.1 mL; 50 mmol) and K_2CO_3 (0.75 g; 5.43 mmol) was dissolved in dry CH_3CN (20 mL) and heated at 45ºC under N_2 atmosphere for 24 h. After cooling to room temperature, the reaction mixture was evaporated under reduced pressure. The black solid was purified by dissolving it in CH_3CN and then precipitating it with hexane. This solid was filtered and washed several times with hexane and diethyl ether.

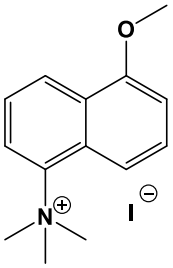

Black solid. Yield: 52% (0.140 g). ^{1}H NMR (DMSO d^6, 400 MHz): δ 8.50 (d, J = 8.5 Hz, 1H), 8.14 (d, J = 8.2 Hz, 1H), 8.12 (d, J = 9.1 Hz, 1H), 7.72 (dd, J = 8.9, 7.9 Hz, 1H), 7.66 (t, J = 8.2 Hz, 1H), 7.22 (d, J = 7.83 Hz, 1H), 4.03 (s, 3H), 3.90 (s, 9H). ^{13}C NMR (DMSO d^6, 101 MHz): 156.45, 141.70, 129.20, 127.70, 125.80, 125.25, 124.60, 121.20, 115.65, 105.90, 57.6, 56.7. HPLC-MS: m/z calc for $C_{14}H_{18}NO^+$ 216.294; found 216.1.

6.5 Study of binding with heparin

Stock solutions of **1**, **2** (5 mM each), and **8** (10 mM) were prepared in DMSO. For all measurements, final sample concentrations were adjusted to 0.05 mM for **1** and **2** and 0.1 mM for **8** using various DMSO-water ratios. A heparin stock solution (25.8 mg/mL) was prepared by dissolving 5.16 mg of heparin in 200 µL of Milli-Q water.

7. CONCLUSIONS

The first objective of this project was to synthesize positively charged achiral molecules, capable of self-assembly upon binding with heparin. Both NDI and naphthalene derivatives were successfully synthesized.

Regarding the second objective, electrostatic interaction between our synthesized positively charged molecules and negatively charged heparin were investigated. The studies revealed that the naphthalene-based compound did not exhibit aggregation, likely due to its limited π-electron cloud. In contrast, the NDI-based compounds did form supramolecular assemblies and exhibited interesting absorption and fluorescence properties. These findings open promising perspectives for potential applications in heparin detection and the development of diagnostic tools.

The supramolecular assemblies formed by the NDI derivatives were induced by the electrostatic interactions with heparin, which facilitated secondary interactions such as π-π stacking and hydrophobic effects, ultimately leading to the formation of self-organized supramolecular complexes.

As for the final objective of this project, the chirality of the helical structures formed was investigated using CD spectroscopy. The results showed that the presence of multiple charges and the extended aromatic core had a significant impact on the induction of chirality. In the case of **2**, a well-defined chiral assembly was formed, whereas in **1**, the CD signal was much weaker. This suggests that the reduced electrostatic interactions and the reduced aromatic core may have limited the formation of the chiral supramolecular structure.

Despite these promising results, the study has certain limitations. For example, the structural characterization of the assemblies could be further complemented by additional techniques such as atomic force microscopy (AFM) or dynamic light scattering (DLS) to confirm the morphology and internal order of the aggregates. Moreover, zeta potential analysis could provide further insights into the nature of electrostatic interactions. NMR analysis of the self-assembly and heparin binding will be crucial to better understand the system.

Future studies should explore a broader range of charged derivatives and systematically vary the number and position of charged groups to better understand their effect on chirality induction and aggregation. Furthermore, these systems may be applied to the selective detection of other biologically relevant polyanions, opening new avenues for supramolecular diagnostics.

8. REFERENCES AND NOTES

1. Aida, T., Meijer, E. W., & Stupp, S. I. (2012). Functional supramolecular polymers. *Science, 335*(6070), 813-817.
2. Sharma, P., Venugopal, A., Verdi, C. M., Roger, M. S., Calò, A., & Kumar, M. (2024). Heparin binding induced supramolecular chirality into the self-assembly of perylenediimide bolaamphiphile. *Journal of Materials Chemistry B. Advance online publication, 12*, 7292-7297.
3. Kumar, M., Brocorens, P., Tonnelé, C., Beljonne, D., Surin, M., & George, S. J. (2014). A dynamic supramolecular polymer with stimuli-responsive handedness. *Nature Communications, 5*, 5793.
4. Kumar, M., Ing, N. L., Narang, V., Wijerathne, N. K., Hochbaum, A. I., & Ulijn, R. V. (2018). Chirality-driven self-assembly of π-conjugated molecules. *Nature Chemistry, 10*, 696-703.
5. Würthner, F. (2004). Control of self-assembly processes of π-conjugated molecules by hydrogen bonding. *Chemical Communications, 14*, 1564-1579.
6. Thomas, S. W., Joly, G. D., & Swager, T. M. (2007). Chemical sensors based on amplifying fluorescent conjugated polymers. *Chemical Reviews, 107*(4), 1339-1386.
7. Molla, M. R., & Ghosh, S. (2012). Orthogonal self-assembly involving hydrogen bonding and π-π stacking interactions. *Physical Chemistry Chemical Physics, 14*(30), 10559-10575.
8. Mukherjee, S., Babarao, R., Desai, A. V., Manna, B., & Ghosh, S. K. (2017). Polar pore surface guided selective CO_2 adsorption in a prefunctionalized metal-organic framework. *Crystal Growth & Design, 17*(7), 3581-3587.
9. Li, F., Huang, Z., Zhou, Q., Pan, M., Tang, Q., & Gong, C. (2020). Energy-saving and long-life electrochromic materials of naphthalene diimide-cored pyridinium salts. *Journal of Materials Chemistry C, 8*(8), 10031-10038.
10. Andric, G., Boas, J. F., Bond, A. M., Fallon, G. D., Ghiggino, K. P., Hogan, C. F., Hutchison, J. A., Lee, M. A.-P., Langford, S. J., Pilbrow, J. R., Troup, G. J., & Woodward, C. P. (2004). Spectroscopy of naphthalene diimides and their anion radicals. *Australian Journal of Chemistry*, *57*(10), 1011-1019.
11. Pérez-Soto, M., Peñalver, P., Street, S. T. G., Weenink, D., O'Hagan, M. P., Ramos-Soriano, J., Jiang, Y. J., Hollingworth, G. J., Galan, M. C., & Morales, J. C. (2022). Structure-activity relationship studies on divalent naphthalene diimide G quadruplex ligands with anticancer and antiparasitic activity. *Bioorganic & Medicinal Chemistry, 71*, 116946.

9. ACRONYMS

δ	Chemical shift
ºC	Degree Celsius
µL	Microliter
^{13}C NMR	Carbon nuclear magnetic resonance
^{1}H NMR	Proton nuclear magnetic resonance
a. u.	Arbitrary units
AFM	Atomic force microscopy
CD	Circular Dichroism
$CDCl_3$	Deuterated chloroform
CH_2Cl_2	Dichloromethane
CH_3CN	Acetonitrile
CH_3I	Iodomethane
d	Doublet
dd	Doublet of doublets
DIPEA	N,N-Diisopropylethylamine
DLS	Dynamic light scattering
DMF	N,N-dimethylformamide
DMSO	Dimethylsulfoxide
DMSO d^6	Deuterated dimethylsulfoxide
eq	Equivalent
EtOH	Ethanol
HPLC-MS	High performance liquid chromatography - mass spectrometry
Hz	Hertz
J	Coupling constant
K_2CO_3	Potassium carbonate
m	Multiplet
mdeg	Millidegree
MeOH	Methanol
mg	Milligram
MHz	Megahertz
mL	Milliliter
mM	Millimolar
mmol	Millimole

N_2	Nitrogen
NDI	Naphthalene diimide
nm	Nanometer
p	Pentuplet
ppm	Parts per million
s	Singlet
t	Triplet
TEM	Transmission electron microscopy
TLC	Thin-layer chromatography
TMS	Tetramethylsilane
UV-Vis	Ultraviolet-visible

APPENDICES

APPENDIX 1: UNSUCCESSFUL REACTIONS

The primary objective of this study was the synthesis of an achiral NDI compound with two positive charges. All the reactions described in this section were expected to proceed via an S_N2 mechanism.

The initial experiments involved reacting compound N,N'-ethylenedimethylamine-decyl-1,4,5,8-naphthalenediimide (9) with bromocholine bromide (10) (Scheme 11). The reactions were performed using various solvents, ethanol (EtOH), DMF and CH_3CN. In each case, the reaction mixtures were subjected to high temperatures: reflux conditions for EtOH and CH_3CN, and 100 °C for DMF. Anhydrous conditions were also applied, using dry solvents and N_2 atmosphere. In all cases, the reactions were allowed to proceed overnight and were subsequently analyzed by HPLC-MS to detect the molecular peak corresponding to the target compound.

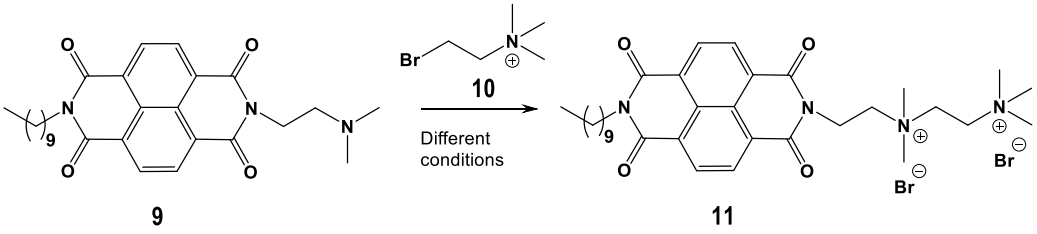

Scheme 11. Synthetic scheme of compound **11**.

None of these conditions, however, yielded the expected product.

To determine whether the limited reactivity could be attributed to the presence of a tertiary amine in **9**, which might reduce its nucleophilicity, a new reaction was conducted using a different reagent, N,N'-ethyleneamonium-hexyl-1,4,5,8-naphthalenediimide (12). This compound was reacted with **10** under reflux in EtOH, in the presence of N,N-Diisopropylethylamine (DIPEA). The addition of DIPEA was essential to deprotonate the amine group of **12** and allow nucleophilic attack.

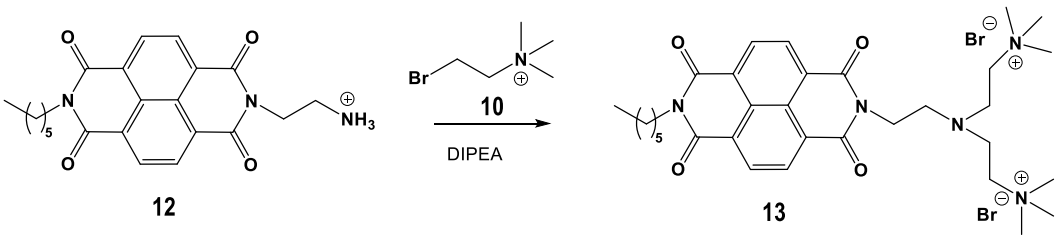

Scheme 12. Synthetic scheme of compound **13**.

Nevertheless, this reaction also failed to produce the desired compound.

These observations suggested that steric hindrance caused by the methyl groups on **10** could be limiting the reaction.

Subsequently, another attempt was made using the reagent N,N'-pyridyl-ethylenamineboc-1,4,5,8-naphthalenediimide (14), which had previously reacted successfully with other bromocholine-like compounds.[11] Due to the presence of a pyridine ring, **14** was expected to show enhanced nucleophilicity and favor product formation. The reaction was carried out in dry DMF at 100 °C under N_2 atmosphere (Scheme 13).

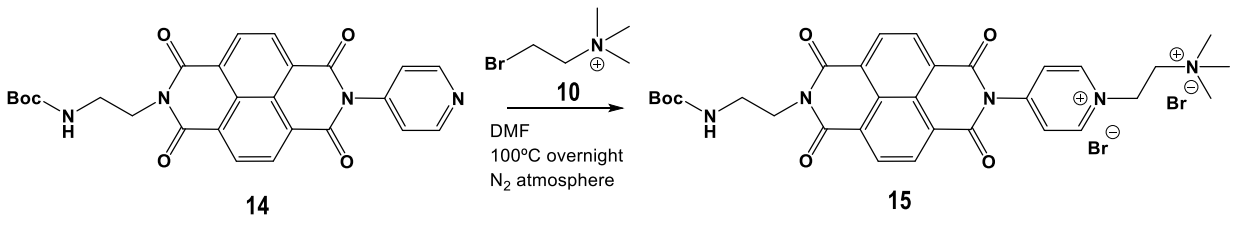

Scheme 13. Synthetic scheme of compound **15**.

Despite these favorable conditions, no formation of the target product was observed.

Given the repeated lack of success, it was hypothesized that **10** itself could be responsible for the reaction failure. To evaluate this, **10** was replaced by an alternative reactant (tert-Butyl (2-bromoethyl)carbamate), and the reaction was repeated with **9** under the same conditions: dry DMF, 100 °C, N_2 atmosphere, and overnight stirring.

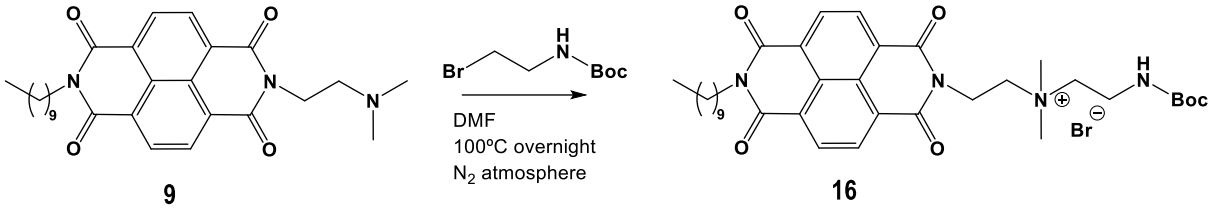

Scheme 14. Synthetic scheme of compound **16**.

Analysis by HPLC-MS revealed the presence of a small amount of the desired product, although in insufficient quantity for isolation and purification. This result suggested that steric hindrance from the Boc group in the reagent, as well as the reduced reactivity of the tertiary amine, could be limiting the reaction.

As an alternative, dibromoethane was tested under identical conditions.

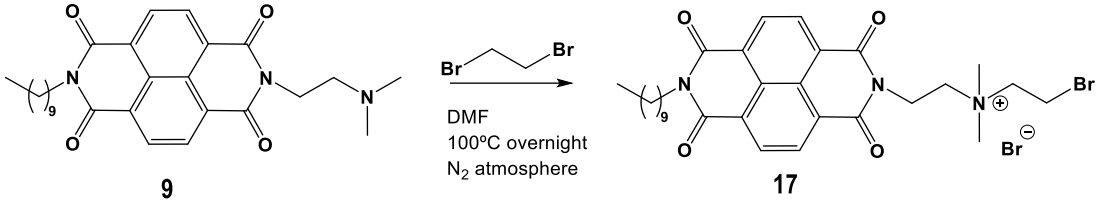

Scheme 15. Synthetic scheme of compound **17**.

In this case, analysis confirmed the formation of the target compound, although the yield remained too low for further work. These findings indicated that **10** might have played an inhibitory role in the previous reactions, as some product formation was detected in both this and the preceding experiment, albeit in limited quantities.

Based on these results, a hypothesis was formulated proposing that **10** could interact unfavorably with the aromatic core of NDI. Specifically, a cation-π interaction was considered, whereby the π electrons of the aromatic rings might interact with the cation group in **10**, leading to the formation of a non-covalent complex that would hinder nucleophilic attack.

To test this hypothesis, ^{1}H NMR experiments were performed. First, the spectrum of pure **10** was recorded in DMSO d^6 to determine the chemical shifts of its protons (Figure 15). Subsequently, a mixture of **9** and **10** was analyzed to identify any changes in the chemical shifts. If a cation-π interaction was present, the protons of **10** would be expected to show increased shielding due to the magnetic anisotropy of the NDI aromatic rings, which induce a local field opposite to the applied magnetic field. Observing such shifts would confirm the interaction and explain the lack of reactivity.

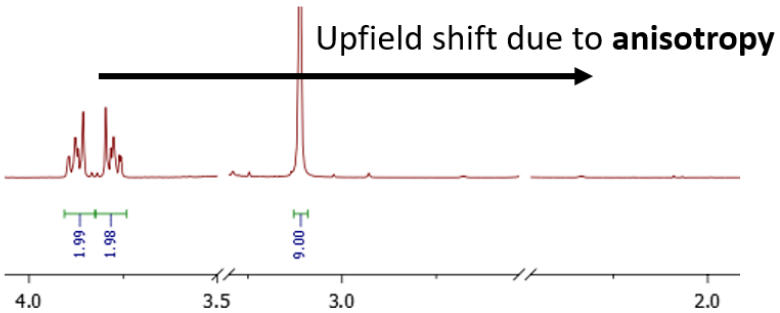

Figure 15. Representation of what would happen to the ^{1}H NMR signals of **10**, if a cation-π interaction was present.

No conclusive results could be obtained, as the mixture of compounds **10** and **9** was not soluble in any of the solvents tested; therefore, the analysis could not be carried out properly.

Consequently, it was concluded that the poor reaction yields were most likely due to the structural characteristics of **10** particularly the presence of a trisubstituted nitrogen bearing methyl groups, which severely hinders S_N2 reactions. Furthermore, as a tertiary amine acting as a nucleophile in reactant **9**, its reactivity is inherently limited by pronounced steric hindrance, which would explain the low product yields observed.

However, the potential involvement of cation-π interactions cannot be ruled out, due to the lack of conclusive results.

APPENDIX 2: SYNTHESIZED COMPOUNDS NMRS

This section presents all the ^{1}H and some ^{13}C NMR spectras of the synthesized compounds.

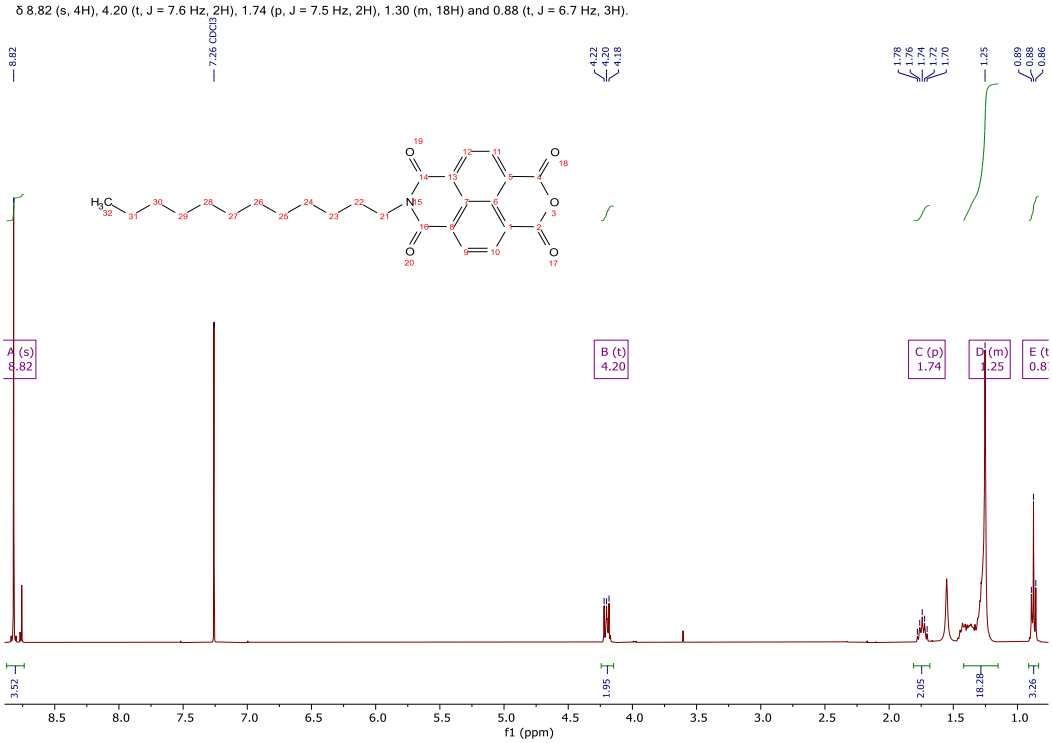

Figure 16. ^{1}H NMR spectra of compound **4** with $CDCl_3$.

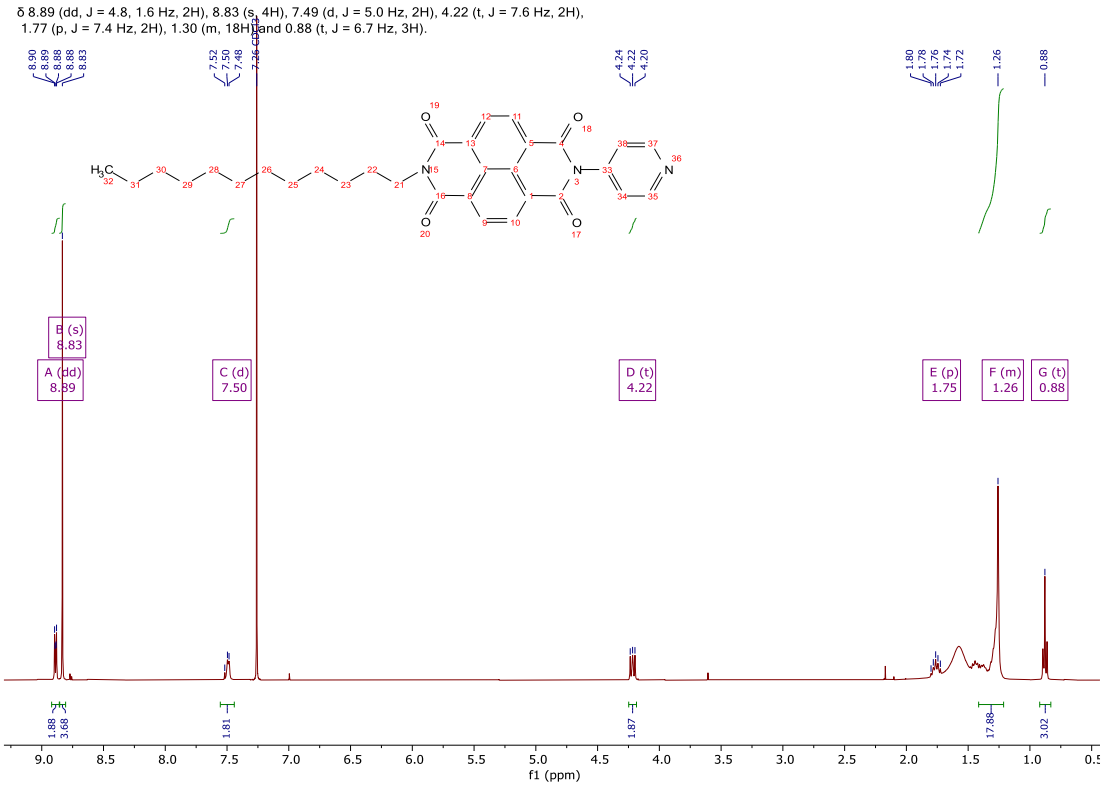

Figure 17. ^{1}H NMR spectra of compound **5** with $CDCl_3$.

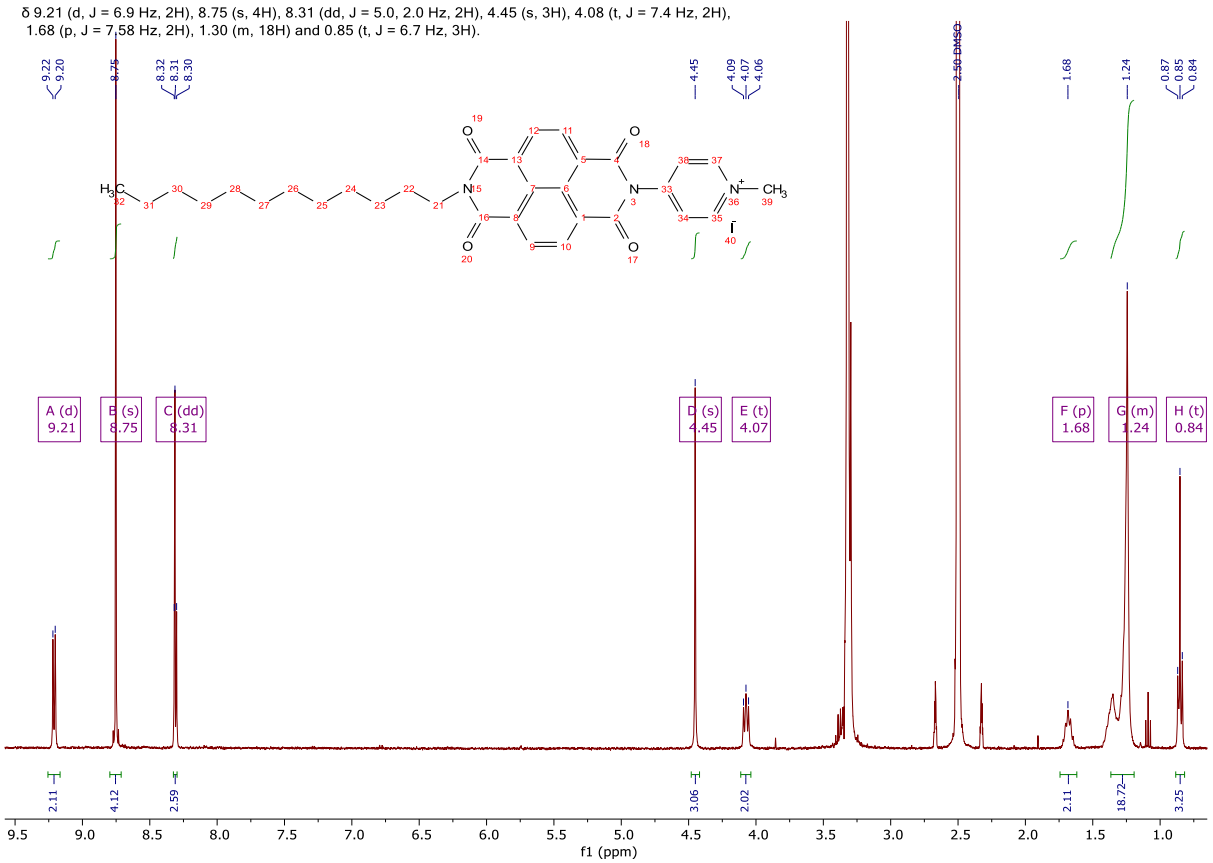

Figure 18. ^{1}H NMR spectra of compound **1** with DMSO d^{6}.

Figure 19. ^{1}H NMR spectra of compound **6** with DMSO d^{6}.

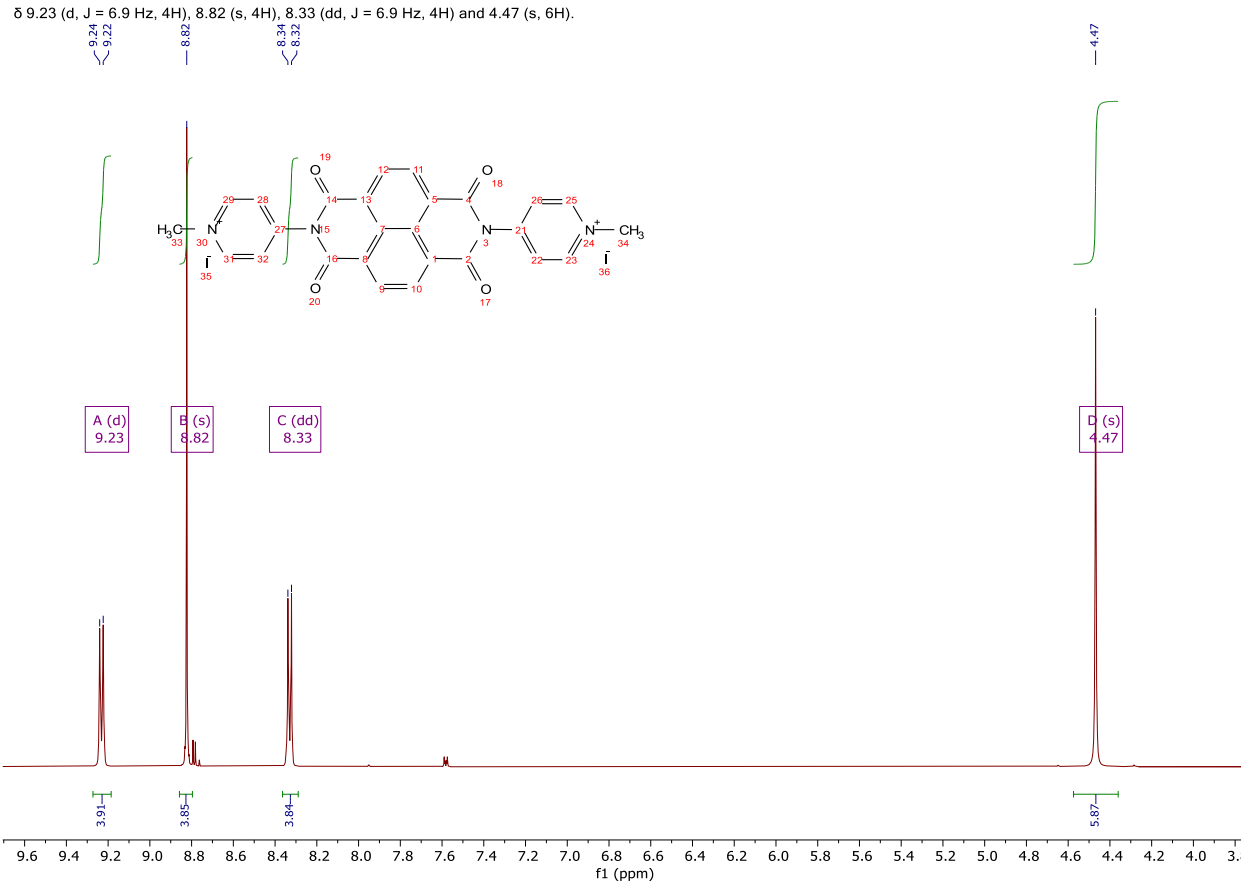

Figure 20. ^{1}H NMR spectra of compound **2** with DMSO d^{6}.

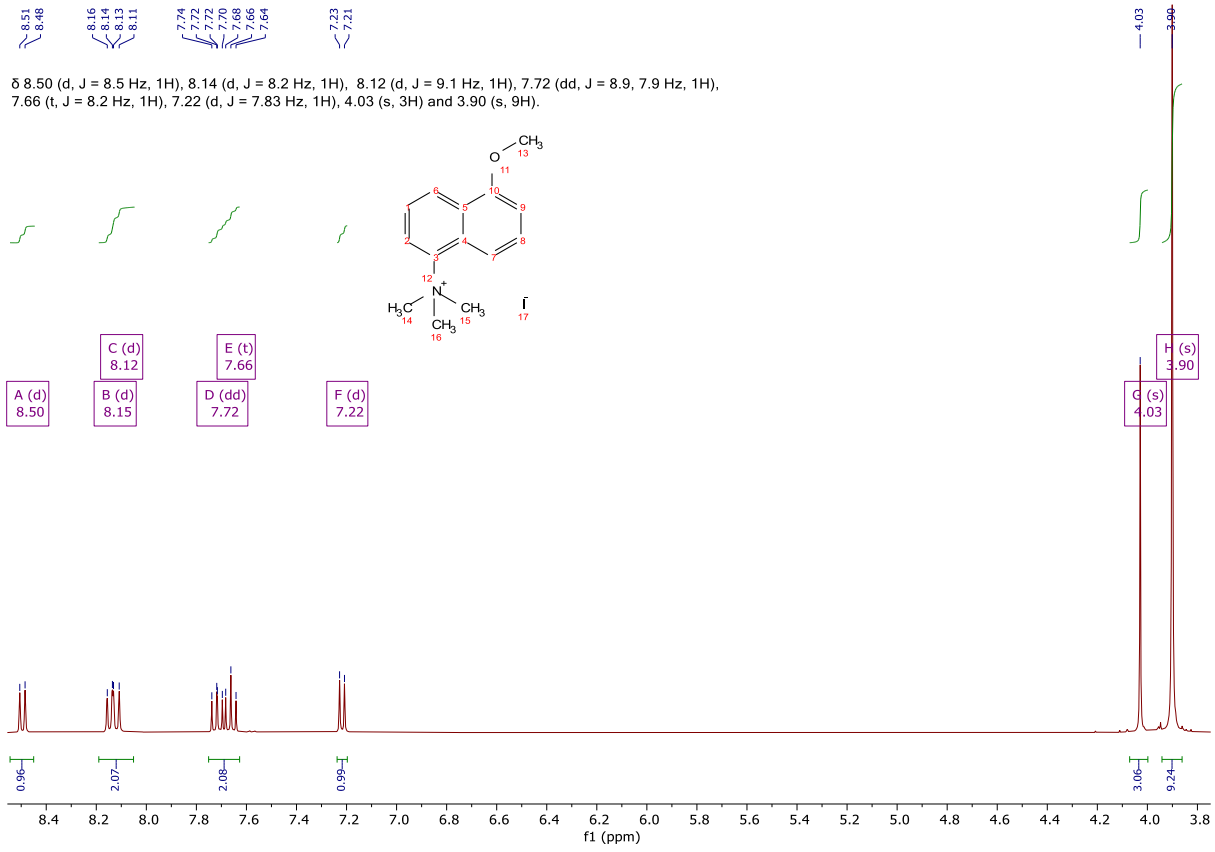

Figure 21. ^{1}H NMR spectra of compound **8** with DMSO d^{6}.

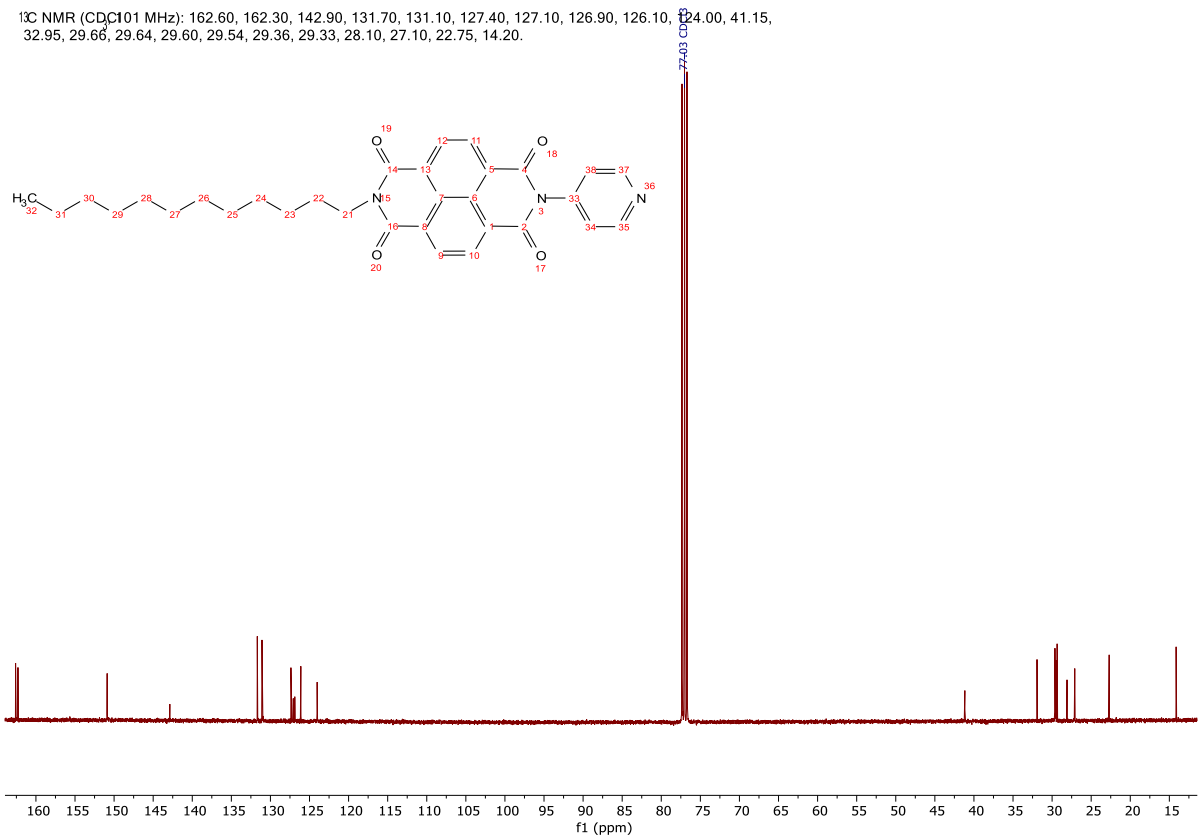

Figure 22. ^{13}C NMR spectra of compound **5** with $CDCl_3$.

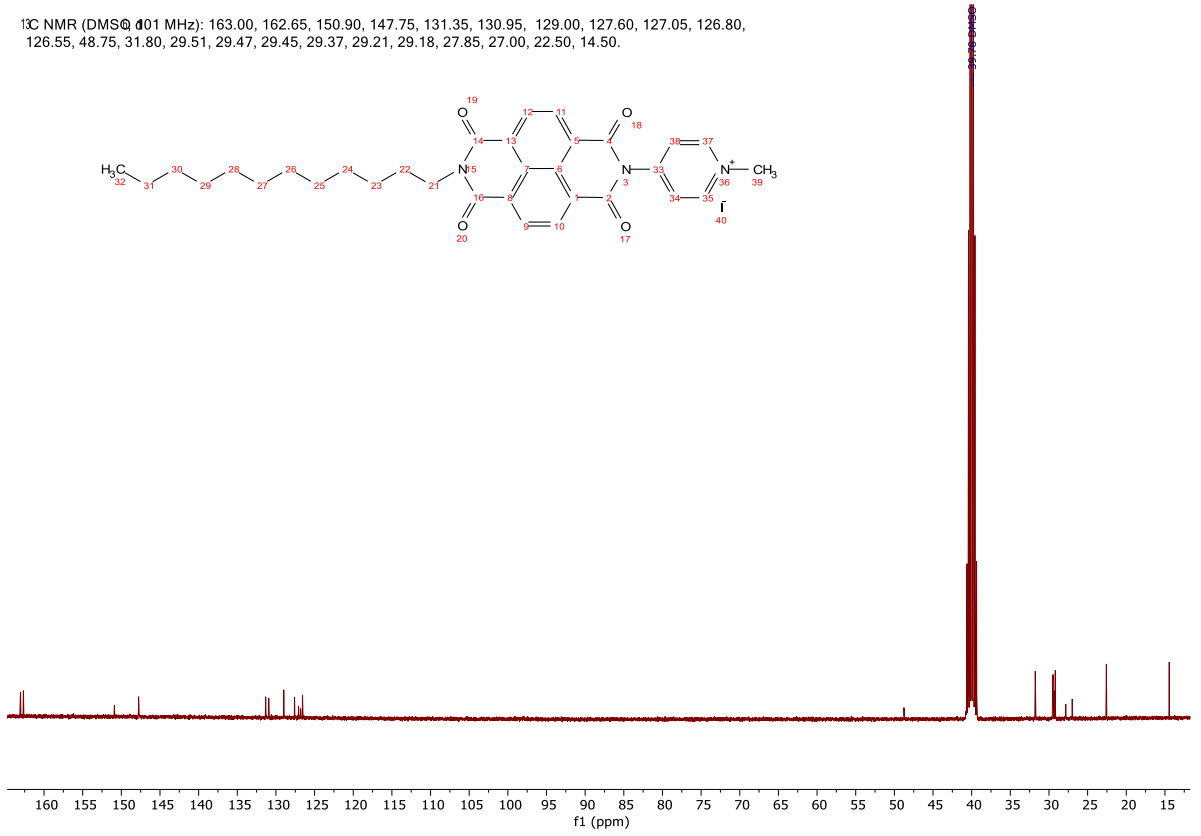

Figure 23. ^{13}C NMR spectra of compound **1** with DMSO d^6.

^{13}C NMR (DMSO, 101 MHz): 156.45, 141.70, 129.20, 127.70, 125.80, 125.25, 124.60, 121.20, 115.65, 105.90, 57.6, 56.7.

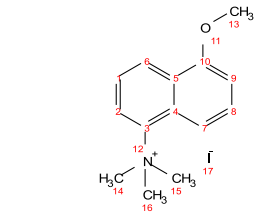

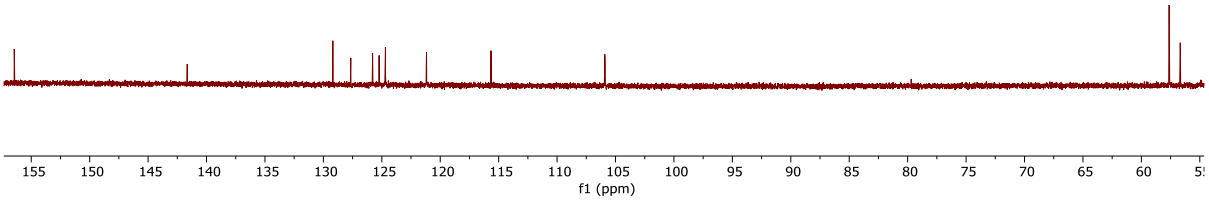

Figure 24. ^{13}C NMR spectra of compound **8** with DMSO d^6.